

Contents lists available at ScienceDirect

Journal of Inorganic Biochemistry

journal homepage: www.elsevier.com/locate/jinorgbio





Oxidation of bisphenol A (BPA) and related compounds by the multifunctional catalytic globin dehaloperoxidase

Dongju Yun, Vesna de Serrano, Reza A. Ghiladi

Department of Chemistry, North Carolina State University, Raleigh, NC 27695-8204, United States

ARTICLE INFO

Keywords:
Bisphenols
Biphenols
Dehaloperoxidase
Hemoglobin
Biodegradation
Peroxidase

ABSTRACT

Dehaloperoxidase (DHP) from the marine polychaete Amphitrite ornata is a multifunctional enzyme that possesses peroxidase, peroxygenase, oxidase and oxygenase activities. Herein, we investigated the reactivity of DHP B with bisphenol A (BPA) and related compounds (bisphenol E, bisphenol F, tetrachlorobisphenol A, 2,2'-biphenol, 3,3'biphenol, 4,4'-biphenol, and 3,3'-dibromo-4,4'-biphenol). As a previously unknown substrate for DHP B, BPA (as a representative substrate) is an endocrine disruptor widely used in polycarbonate and epoxy resins, thus resulting in human exposure. Reactivity studies with these substrates were investigated using high performance liquid chromatography (HPLC), and their corresponding oxidation products were determined by mass spectrometry (GC-MS/ LC-MS). BPA undergoes oxidation in the presence of DHP B and hydrogen peroxide yielding two cleavage products (4-isopropenylphenol and 4-(2-hydroxypropan-2-yl)phenol), and oligomers with varying degrees of oxidation. ¹⁸O-labeling studies confirmed that the O-atom incorporated into the products was derived exclusively from water, consistent with substrate oxidation via a peroxidase-based mechanism. The X-ray crystal structures of DHP bound with bisphenol E (1.48 Å), bisphenol F (1.75 Å), 2,2'-biphenol (1.90 Å) and 3,3'biphenol (1.30 Å) showed substrate binding sites are in the distal pocket of the heme cofactor, similar to other previously studied DHP substrates. Stopped-flow UV-visible spectroscopy was utilized to investigate the mechanistic details and enzyme oxidation states during substrate turnover, and a reaction mechanism is proposed. The data presented here strongly suggest that DHP B can catalyze the oxidation of bisphenols and biphenols, thus providing evidence of how infaunal invertebrates can contribute to the biotransformation of these marine pollutants.

1. Introduction

Bisphenol A (BPA) is a synthetic chemical compound widely used industrially as a material for polycarbonate plastics and epoxy resins due to its high temperature resistance [1]. It has also been used as a component in insecticides, in sealants and composites in dentistry, and as a protective coating for metal food container and baby bottles, among others. Because of the extensive commercial usage of products containing BPA, it has been frequently detected in lakes, drinking water, beverages and food [2,3]. BPA has been classified as an endocrine

disrupting chemical (EDC) by the World Wide Fund for Nature (WWF) and the United States Environmental Protection Agency (EPA) [4]. These endocrine disrupting chemicals interfere with hormones of animals and humans due to their structural resemblance to natural estrogen, and they can lead to prostate cancers, decreased sperm count, sexual dysfunction, reproductive problems and early puberty [5,6]. Therefore, there has been rising concern about the potential threats of BPA to both human health and the environment.

In recent years, diverse methods have been proposed to degrade BPA, such as Fenton and Fenton-like processes [7,8], ozonation [9,10],

Abbreviations: Abbreviation, Explanation; DHP, dehaloperoxidase; HRP, horseradish peroxidase; HSM, horse skeletal muscle; Mb, myoglobin; WT, wild-type; BPA, Bisphenol A; BPE, Bisphenol E; BPF, Bisphenol F; TBP, 2,4,6-tribromophenol; TCP, 2,4,6-trichlorophenol; DMPO, 5,5-dimethyl-1-pyrroline N-oxide; DMSO, dimethyl sulfoxide; EI, electron ionization; ESI, electrospray ionization; PDB, protein data back; Compound I, two-electron oxidized heme cofactor compared to the ferric form, commonly as an Fe^{IV} \equiv O porphyrin π-cation radical; Compound II, one-electron oxidized heme cofactor when compared to the ferric form, commonly as an Fe^{IV} \equiv O or Fe^{IV} \equiv OH; Compound ES, two-electron-oxidized state containing both a ferryl center [Fe^{IV} \equiv O] and a tyrosyl radical, analogous to Compound ES in cytochrome c peroxidase; Compound RH, 'reversible heme' state of dehaloperoxidase, formed from the decay of Compound ES in the absence of co-substrate.

* Corresponding author.

E-mail address: Reza_Ghiladi@ncsu.edu (R.A. Ghiladi).

photocatalysis [11], electrocatalytic oxidation [12] and biological degradation [13–15]. Among them, biodegradation has received much attention since a variety of organisms from microorganisms to mammals have been reported to decompose BPA [16]. Although biodegradation of BPA has been extensively studied with microorganisms or plants, there is very little information with regards to its biotransformation by marine invertebrates.

Our chosen platform for the biodegradation of BPA is the benthic marine invertebrate Amphitrite ornata [17]. This segmented infaunal organism coinhabits coastal mudflats with other organisms that secret toxic halogenated metabolites (including bromophenols, bromoindoles, and bromopyrroles) as chemical defense mechanisms [18-20]. A. ornata employs its hemoglobin, named dehaloperoxidase (DHP), as a detoxifying agent to survive in such harsh environments by performing the oxidation of marine pollutants that are produced by other organisms [21-24]. Utilizing this natural phenomenon, studies on DHP have focused on its reaction with toxic single ring phenolic compounds that are produced either naturally or from anthropogenic sources [25-32], which can potentially contaminate marine environments. It has been shown that DHP is a multifunctional hemoglobin that catalyzes the oxidation of a wide variety of substrates, including halophenols [25,26,33], nitrophenols [27], haloindoles [28], guaiacols [29] and cresols [30]. The substrate oxidation reactions by DHP proceed via 4 different biologically relevant activities: peroxidase [24,26,30,33-35], peroxygenase [27,28,30,32], oxidase [28], and oxygenase [36]. The catalytic cycle of dehaloperoxidase follows the general one proposed by Poulos and Kraut [37,38] for heme peroxidases in that ferric DHP is activated by hydrogen peroxide to ferryl-containing species [39], either as Compound I [(Por +)Fe^{IV}=O AA] (AA = amino acid) [40,41] or Compound ES [(Por)Fe^{IV}=O AA•] [33]. These reactive iron-oxo species oxidize substrate with concomitant formation of the resting ferric state, whereas in the absence of substrate, Compound RH, an inactive form of DHP, is observed [33,42,43]. Most of the substrates studied with DHP were crystallographically observed to bind in the distal heme pocket [24,44,45]. To date, however, it is still not known the limitation of the size of molecules that DHP B can accommodate (and catalyze the oxidation of) within its active site, particularly with respect to multi-ring phenolic compounds.

Here, we present structural, spectroscopic, and mechanistic studies describing the reactivity of bisphenols (BPA, bisphenol E, bisphenol F and tetrachlorobisphenol A) and biphenols (2,2'-biphenol, 3,3'-biphenol, 4,4'-biphenol and 3,3'-dibromo-4,4'-biphenol) with the multifunctional catalytic globin dehaloperoxidase, and establish BPA and related compounds as new substrates for DHP. As shown in Fig. 1, these new substrates are double-ring phenols, which are larger than the previously studied single-ring phenolic substrates, and further confirm the plasticity of the DHP active site for accommodating a wide scope of substrate with varying sizes. The results here will demonstrate that DHP has a broader potential as a multifunctional protein toward phenolic

contaminants than previously shown. Moreover, given that BPA and related compounds are widely used in industry and are known marine contaminants, this study demonstrates how these pollutants, either directly or indirectly (through their degradation or biotransformations resulting in metabolites), may be impacted by, or can potentially impact, infaunal invertebrates and other marine organisms through their reactivity with marine hemoglobins.

2. Experimental

2.1. Materials and methods

Ferric WT DHP B was expressed and purified as previously reported [26,46]. Oxyferrous DHP B was prepared by the aerobic addition of excess ascorbic acid to ferric DHP B, followed by desalting (PD-10 column) to remove the leftover reducing agent [47]. The enzyme concentrations were determined spectrophotometrically using the known molar absorptivities of the Soret band (ϵ_{Soret}): WT DHP ($\epsilon_{Soret} = 116,\!400$ M^{-1} cm⁻¹ [26]), horse skeletal muscle (HSM) myoglobin (ε_{Soret} = 188,000 M⁻¹ cm⁻¹ [48]) and horseradish peroxidase (HRP) (ε_{Soret} = $102,000~\mathrm{M}^{-1}~\mathrm{cm}^{-1}$ [49]). HSM and HRP were purchased from Sigma-Aldrich and used as received. Substrate stock solutions (10 mM) were prepared in methanol and stored at -80 °C until needed. Solutions of H₂O₂ were prepared fresh daily in 100 mM KP_i and kept on ice until needed. Isotopically labeled H₂¹⁸O₂ (90% ¹⁸O-enriched) and H₂¹⁸O (98% ¹⁸O-enriched) were purchased from Icon Isotopes (Summit, NJ). Acetonitrile (MeCN) was high-performance liquid chromatography (HPLC) grade, and all other reagent-grade chemicals were purchased from VWR, Sigma-Aldrich or Fisher Scientific and used without further purification.

2.2. HPLC reactivity studies

Reactions were performed in triplicate in 100 mM KP_i containing 5% MeOH at room temperature. A typical reaction (250 μL final volume) was initiated by the addition of 500 µM H₂O₂ to a 100 mM KP_i (pH 7) solution containing 10 μM enzyme and 500 μM substrate, and quenched after 5 min with an excess of catalase. Enzyme variants included ferric WT DHP B, ferric DHP B (Y28F/Y38F) [41], oxyferrous WT DHP B, ferric WT DHP A, HSM and HRP. Mechanistic probes were added prior to the addition of H_2O_2 , including 500 μM 4-bromophenol (MeOH), 500 μM Dmannitol (100 mM KPi), 100 mM 5,5-dimethyl-1-pyrroline N-oxide (DMPO, in MeOH) or 10% v/v dimethyl sulfoxide (DMSO), and adjustments were made to ensure a final 5% MeOH concentration for all reactions except DMPO (10% MeOH final). A 200 µL aliquot of the reaction mixture was diluted 4-fold with 600 μL distilled water, and the diluted samples were analyzed using a Waters e2695 Separations Module coupled to a Waters 2998 photodiode array detector and equipped with a Thermo Fisher Scientific ODS Hypersil (150 \times 4.6 mm)

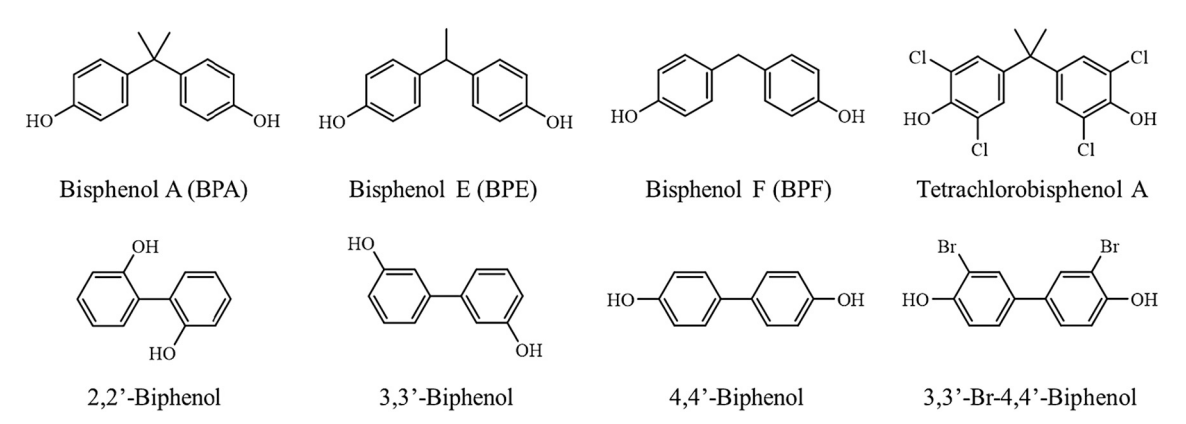


Fig. 1. Bisphenol A (BPA) and related compounds investigated for enzyme-catalyzed oxidation by DHP B in the presence of hydrogen peroxide.

 $5~\mu m$ particle size C_{18} column. Separation was performed using a linear gradient of binary solvents (solvent A, water +0.1% TFA; solvent B, acetonitrile +0.1% TFA). The elution consisted of the following conditions: (1.5 mL/min A:B) 95:5 to 5:95 using a linear gradient over 11 min, 5:95 isocratic for 3 min, 5:95 to 95:5 using a linear gradient over 1 min, and then isocratic for 3 min. Data analysis was performed using the Waters Empower software package.

2.3. Product determination by liquid chromatography mass spectrometry (LC-MS)

The reactions (250 µL final volume) were performed by the addition of 500 μM H₂O₂ to a solution containing 10 μM enzyme and 500 μM substrate in 1 mM NH₄OAc buffer at pH 7 or 8, and quenched after 10 min with an excess of catalase. For the $^{18}\mathrm{O}$ labeling studies, the reactions were performed for 10 min in the presence of DHP B, substrate, and H_2O_2 , where unlabeled H_2O_2 was replaced with $H_2^{18}O_2$, and/or the 1 mM NH₄OAc buffer was replaced with H₂¹⁸O to ensure >90% of labeled ¹⁸O was present. Analysis of the undiluted reaction (20 µL injection aliquot) was carried out using a Thermo Fisher Scientific Exactive Plus Orbitrap mass spectrometer employing a heated electrospray ionization (HESI) probe and equipped with a Thermo Hypersil Gold (50 \times 2.1 mm, particle size 1.9 μm) C₄ column. The flow rate was set to 250 μL/min (solvent A, water +0.1% formic acid; solvent B, acetonitrile +0.1% formic acid) and the mass spectrometer was operated in negative ion mode to yield [M-H] species. Spectra were collected while scanning from 100 to 1500 m/ z and data analysis was performed using Thermo Xcalibur software.

2.4. Product determination by gas chromatography mass spectrometry (GC-MS)

The reactions (1 mL final volume) were performed by the addition of 500 $\mu M~H_2O_2$ to a solution containing 10 μM enzyme and 500 μM substrate in 100 mM KPi buffer at pH 8, and quenched after 10 min with 500 µL ethyl acetate (EtOAc). After the mixture was vortexed for 10 s, the organic phase was collected in a centrifuge. A second extraction was conducted with an additional 500 µL EtOAc, and the organic phases were combined and dried over anhydrous Na₂SO₄. For the ¹⁸O labeling studies, the reactions were performed in the same manner, but in three different conditions: i) $H_2^{18}O/H_2O_2$, ii) $H_2O/H_2^{18}O_2$ and iii) $H_2^{18}O/H_2^{18}O_2$, where unlabeled H₂O₂ was replaced with H₂¹⁸O₂, and/or buffer was replaced with H₂¹⁸O to ensure >90% of labeled ¹⁸O was present. Analysis was carried out using an Agilent 8860 GC system equipped with an Agilent 19091S—433B HP-5MS UI (Ultra Inert) column (30 m × 0.250 mm, 0.25 µm film thickness) coupled with a 5977B GC/MSD equipped with an electron ionization (EI) detector. The following method was utilized: initial temperature was held at 50 °C for 9 min, ramped at 5 °C/ min to 240 °C and held for 12 min (total run time: 59 min); 250 °C inlet temperature, 275 °C detector temperature, 1 µL injection volume, 1 mL/ min flow rate He carrier gas.

2.5. Binding studies

The substrate dissociation constants (K_d values) were determined in triplicate for ferric WT DHP B in 100 mM KP_i (pH 7) containing 5% MeOH at room temperature using a Cary 50 UV–vis spectrophotometer using previously published protocols [28,50]. The UV–vis spectrometer was referenced with 25 μ M WT DHP B in 100 mM KP_i (pH 7) with 5% MeOH. Spectra were acquired in the presence of substrate (1–200 equiv) while constant DHP B (25 μ M) and methanol concentrations were maintained. Analysis of the Q-band region (450–650 nm) was performed using the ligand binding function in Grafit (Erithacus Software Ltd.).

2.6. Stopped-flow UV-visible spectroscopic studies

All solutions were prepared in 100 mM KP_i (pH 8), and adjustments

were made to ensure a final 5% MeOH concentration for all reactions. Experiments were performed as follows: i) For single-mixing experiments, enzyme [ferric DHP B(Y28F/Y38F), ferric DHP B or oxyferrous DHP B] that was pre-incubated with 20 equiv. of BPA was then reacted with 10 equiv. of H₂O₂, and ii) double-mixing experiments were conducted using an aging line prior to the second mixing step to observe Compound I/ES/II reactivity with 20 equiv. substrate, as follows: (a) Compound I was pre-formed from the reaction of ferric DHP B(Y28F/ Y38F) [41] with 10 equiv. H₂O₂ in an aging line for 70 ms prior to mixing with the substrate; (b) Compound ES was pre-formed by reaction of ferric WT DHP B with 10 equiv. of H₂O₂ in an aging line for 433 ms prior to mixing with the substrate [26]; and (c) Compound II was preformed from oxyferrous DHP B that was pre-incubated with 1 equiv. TCP and then reacted with 10 equiv. of H₂O₂ in an aging line for 7.84 s prior to mixing with the substrate [29,47]. Aging times were determined by single-mixing experiments.

Optical spectra were recorded using a Bio-Logic SFM-400 triple-mixing stopped-flow instrument coupled to a rapid scanning (1.5 ms) diode array UV — vis spectrophotometer. Data were collected (900 scans total) over a three-time domain (1.5, 15 and 150 ms/15, 150, and 1500 ms) observation period using the Bio-Kine 32 software package (Bio-Logic). All data were evaluated using the Specfit Global Analysis System software package (Spectrum Software Associates) and fit with SVD analysis as one-step/two-species, two-step/three-species or three-step/four species irreversible mechanisms, where applicable. For data that did not properly fit these models, experimentally obtained spectra at selected time points detailed in the figure legends are shown. Data were baseline-corrected using the Specfit autozero function.

2.7. Protein crystallization and X-ray diffraction studies

In order to crystallize the protein, DHP B was expressed in non-His tagged form, and was purified according to established procedures [29]. Prior to crystallization, the protein was oxidized to the ferric form, and concentrated to 12 mg/mL. DHP was crystallized by the hangingdrop vapor diffusion method from a solution consisting of 29-32% MPEG 2000 or MPEG 5000, 0.2 M ammonium sulfate and 20 mM sodium cacodylate (pH 6.5), and the crystallization drops were set up by mixing protein and crystallizing solutions at 1:1, 1.5:1 and 2:1 volume ratios. Crystals grew within 3-5 days of incubation at 4 °C, and were subsequently incubated with substrates by soaking in crystallizing solution supplemented with substrate dissolved in DMSO, with a final DMSO concentration of 5% in the soaking solution and final substrate concentrations from 10 to 40 mM. After an overnight soaking at 4 °C, the crystals were briefly immersed in a cryoprotection solution consisting of 25% glycerol supplemented crystallization solution, and were cryocooled by plunging into liquid nitrogen. The measurements of the crystal diffraction were performed remotely on the 22-BM beam line of SER-CAT operated by Advanced Photon Source, Argonne National Laboratories. The diffraction data were collected at 100 K, using a wavelength of 1.00 Å, and employing a Rayonix MX300HS detector at a crystal-to-detector distance of 150 mm.

The diffraction data were processed with HKL2000 and XDS software packages [51,52]. The structures of the complexes were solved by molecular replacement with Phaser [53] using PDB 3IXF coordinates as a starting model [46]. The resulting models were refined using Refmac5 from the CCP4 suite [54,55] and phenix.refine from the Phenix suite of programs [56,57] and inspection and manual model building was performed in COOT [58]. Final models were validated using COOT and MolProbity [59]. Figures were generated using PyMol (Schrodinger).

3. Results and discussion

3.1. DHP-catalyzed substrate reactivity with H₂O₂

3.1.1. Substrate variation

The hydrogen peroxide-dependent oxidation reaction of ferric DHP B with bisphenol A (BPA) and related compounds was monitored via HPLC, and the corresponding substrate conversion percentages (based upon substrate loss) are listed in Table 1. Reactions were initiated upon addition of 500 μM of H_2O_2 to a pH 7 buffer solution containing 10 μM enzyme and 500 μM substrate, incubated at 25 $^{\circ} C$ for 5 min, and then quenched with an excess of catalase. Substrate oxidations ranged from a low value of 7.6% for tetrachlorobisphenol A to a high of 87.1% for 2,2'biphenol. The low oxidation % conversion of tetrachlorobisphenol A is likely due to the steric hindrance effect, where the halogen atom at the ortho-position strongly inhibits the oxidation of the phenolic C-OH [60,61]. No substrate turnover was observed when either DHP (nonenzymatic control) or peroxide (non-oxidant control) were excluded from the reaction for 7 substrates (data not shown); however, some reactivity was observed for 3,3'-dibromo-4,4'-biphenol in the absence of hydrogen peroxide, but this was not investigated further given its low background level (7.8 \pm 6.8%).

3.1.2. Optimization studies

Using BPA as a representative substrate, the following optimization studies were conducted (Table 2): (i) pH optimization: the oxidation of BPA was performed from pH 5-9, with a \sim 2-fold increase in substrate oxidation observed as the reaction pH was increased from 5 (37.1%) to 8 (72.9%), but decreased at pH 9 (53.7%). (ii) Temperature optimization: the effect of temperature on the oxidation activity of the enzyme for BPA was investigated at 0, 25, 37 and 50 °C, with a maximum value for substrate conversion achieved at 25 $^{\circ}$ C (68.8%). (iii) H_2O_2 optimization: the optimum concentration of H2O2 for the oxidation of BPA was determined using various concentrations of H_2O_2 (50, 100, 250, 500 μM and 1000 μ M), with maximal conversion at 500 μ M H₂O₂ (68.8%), with no significant increase above that value. (iv) Reaction time optimization: the effect of different incubation times on the oxidation of BPA was studied by conducting experiments from 30 s to 30 min, where it was found that substrate conversion increased until 10 min reaction time (73.0%), at which point it reached a plateau. Taken together, the optimized reaction conditions for BPA were determined to be: [ferric DHP B] = 10 μM, [substrate] = $[H_2O_2]$ = 500 μM, 5% MeOH/100 mM KP_i (ν / v) at pH 8, 25 °C, 10 min. When the substrate oxidation studies were repeated under the optimized conditions, the substrate conversions were increased 1.2-3.4 fold, with the one exception being 2,2'-biphenol (Table 1), which is likely due to the fact that only 2,2'-biphenol has a pKa value lower than pH 8 among the substrates studied (pKa values: BPA, 9.78-10.39 [62]; bisphenol E, 9.81-10.42 [62]; bisphenol F, 9.84-10.45 [62]; 2,2'-biphenol, 7.6 [63]; 4,4'-biphenol, 9.7 [63]).

Table 1
DHP-catalyzed oxidation of BPA and related compounds.

Substrate	Conversion (%)			
DHP B WT Ferric	pH 7, 5 min	pH 8, 10 min		
+ Bisphenol A	68.8 ± 2.9	86.0 ± 1.0		
+ Bisphenol E	63.2 ± 1.6	79.2 ± 1.0		
+ Bisphenol F	72.2 ± 3.1	82.7 ± 1.7		
+ Tetrachlorobisphenol A	7.6 ± 3.4	25.6 ± 5.9		
+ 2,2'-Biphenol	87.1 ± 5.3	64.0 ± 3.6		
+ 3,3'-Biphenol	24.0 ± 2.9	39.8 ± 0.9		
+ 4,4'-Biphenol	55.0 ± 7.9	83.0 ± 1.2		
+ 3,3'-Dibromo-4,4'-biphenol	14.8 ± 6.7	17.7 ± 5.5		

Reaction conditions: [ferric DHP B] = 10 μ M, [substrate] = [H₂O₂] = 500 μ M, 5% MeOH/100 mM KP_i (ν / ν) at room temperature.

 Table 2

 Reaction optimization studies for the oxidation of BPA.

Condition	Conversion (%)	Condition	Conversion (%)	
pH studies		H ₂ O ₂ studies		
pH 5.0	37.1 ± 1.4	50 μM	25.3 ± 1.4	
pH 6.0	45.0 ± 2.9	100 μΜ	44.4 ± 3.3	
pH 7.0	68.8 ± 2.9	250 μΜ	60.9 ± 2.4	
$-H_2O_2$	n.d.	500 μM	68.8 ± 2.9	
-Enzyme	n.d.	1000 μΜ	65.3 ± 2.2	
pH 8.0	72.9 ± 0.7	Reaction time studies		
pH 9.0	53.7 ± 0.9	30 s	38.4 ± 1.5	
Temperature studies		1 min	49.7 ± 1.9	
0 °C	53.8 ± 1.6	2 min 30 s	62.5 ± 0.3	
25 °C	68.8 ± 2.9	5 min	68.8 ± 2.9	
37 °C	41.5 ± 3.1	10 min	73.0 ± 1.0	
50 °C	24.1 ± 0.4	30 min	$\textbf{74.2} \pm \textbf{0.6}$	

Reaction conditions: [ferric DHP B] = 10 μ M, [BPA] = 500 μ M, 5% MeOH/100 mM KP_i (ν / ν), [H₂O₂] = 500 μ M, pH 7, 25 °C, 5 min (unless otherwise indicated); n.d.= no reactivity detected.

3.1.3. Enzyme variation

The enzyme variation and mechanistic investigations with BPA were performed under both unoptimized and optimized conditions, and the results are summarized in Table 3. Nearly the same amount of BPA conversion was observed when initiating BPA oxidation with oxyferrous WT DHP B (69.2%) as with the ferric form (68.8%) under unoptimized conditions. The oxidation of BPA was slightly attenuated for oxyferrous DHP B (78.1%) compared to the ferric enzyme (86.0%) under optimized conditions, but still demonstrated that the substrate oxidation reaction can be initiated from either the oxyferrous ("hemoglobin-like") or ferric ("peroxidase-like") oxidation states, a result consistent with previous literature studies [25,27-29,32,43,47]. The mutant DHP B (Y28F/ Y38F), which forms Compound I as the initial reactive intermediate rather than the Compound ES species observed in WT DHP B [41], showed ~1.1-1.2 fold more activity (81.6% unoptimized, 92.9% optimized) compared to WT DHP B (68.8%, 86.0%). DHP isoenzyme A (58.5%, 55.5%), which differs from DHP B (68.8%, 86.0%) by only five amino acid substitutions [26,46,64], showed a lower conversion. The lower activity of isoenzyme A over that of B has also been observed previously with tribromophenol (TBP) and trichlorophenol (TCP) [26] (peroxidase activity), as well as 5-Br-indole [28], 4-nitrophenol and 2,4dinitrophenol [27] (peroxygenase activity). Finally, the canonical horseradish peroxidase (HRP) yielded 1.1-1.4 fold higher conversion (99.3%, 96.4%) of BPA and horse skeletal muscle myoglobin (HSM Mb) showed ~2.9-fold lower conversion (23.6%, 29.6%) compared to WT DHP B (68.8%, 86.0%). These results support that DHP reactivity with BPA is comparable with those of classical peroxidase enzymes but is greater than those of other members of the globin family.

Table 3DHP-catalyzed oxidation of BPA as a function of enzyme variant and mechanistic probes.

Condition	Conversion (%)	Conversion (%)		
Enzyme Variation	pH 7, 5 min	pH 8, 10 min		
DHP B Ferric	68.8 ± 2.9	86.0 ± 1.0		
DHP B Oxyferrous	69.2 ± 0.8	78.1 ± 6.4		
DHP B (Y28F/Y38F)	81.6 ± 0.9	92.9 ± 0.5		
DHP A Ferric	58.5 ± 0.8	55.5 ± 1.0		
HRP	99.3 ± 0.05	96.4 ± 2.1		
HSM Mb	23.6 ± 1.1	29.6 ± 4.3		
Mechanistic Probes				
500 mM p-mannitol	67.2 ± 1.6	84.6 ± 0.9		
10% DMSO	60.3 ± 1.3	62.4 ± 0.5		
100 mM DMPO	49.2 ± 1.4	50.9 ± 2.5		
500 mM 4-bromophenol	11.9 ± 6.9	39.2 ± 8.8		

Reaction conditions: [Enzyme] = 10 μ M, [BPA] = [H₂O₂] = 500 μ M, 5% MeOH/ 100 mM KP_i (ν /v) at pH 7 or 8, 25 °C, 5 or 10 min.

3.1.4. Mechanistic studies

The BPA oxidation reaction was performed in the presence of the known radical scavengers [p-mannitol, dimethyl sulfoxide (DMSO), and 5,5-dimethyl-1-pyrroline N-oxide (DMPO)]. While the presence of p-mannitol (67.2%, 84.6%) did not show a significant change in substrate conversion, the addition of DMSO (60.3%, 62.4%) and DMPO (49.2%, 50.9%) exhibited 1.1–1.7 fold losses in activity when compared to the reaction in their absence (68.8%, 86.0%). No changes in product distribution were observed by HPLC in the presence of these radical scavengers (data not shown). The addition of 4-bromophenol ($K_d = 1.15 \text{ mM}$ [65]), a known peroxidase and peroxygenase inhibitor [66,67], decreased substrate conversion by 2.2–5.8 fold, suggesting that 4-bromophenol has an inhibitory effect on BPA oxidation.

3.2. Identification of reaction products

A representative chromatogram for each ferric DHP B-catalyzed substrate oxidation reaction in the presence of H_2O_2 is shown in Fig. 2. The oxidation reactions were further analyzed by LC-MS (negative ion mode [M-H] $^-$), and lists of the products with their retention times, masses and chemical formulae obtained can be found in Tables S1 and S2. Under the conditions employed, multiple products were observed, and although identification of the exact chemical structures of all products was not pursued, they consisted of different monomers and oligomers (up to n=4) with varying degrees of oxidation.

As a representative substrate, BPA was further investigated for product identification. For this work, GC–MS and LC-MS (negative ion mode [M-H] $^-$) techniques were used to identify products formed in the DHP-catalyzed BPA oxidation reaction. As shown in Tables 4, 4-iso-propenylphenol and 4-(2-hydroxypropan-2-yl)phenol were two cleavage products identified from the reaction sample by GC–MS: the product that exhibited a retention time (t_R) at 24.3 min also showed an identical mass fragmentation pattern [134(100), 119(80.6), 105(8.7), 91(30.2),

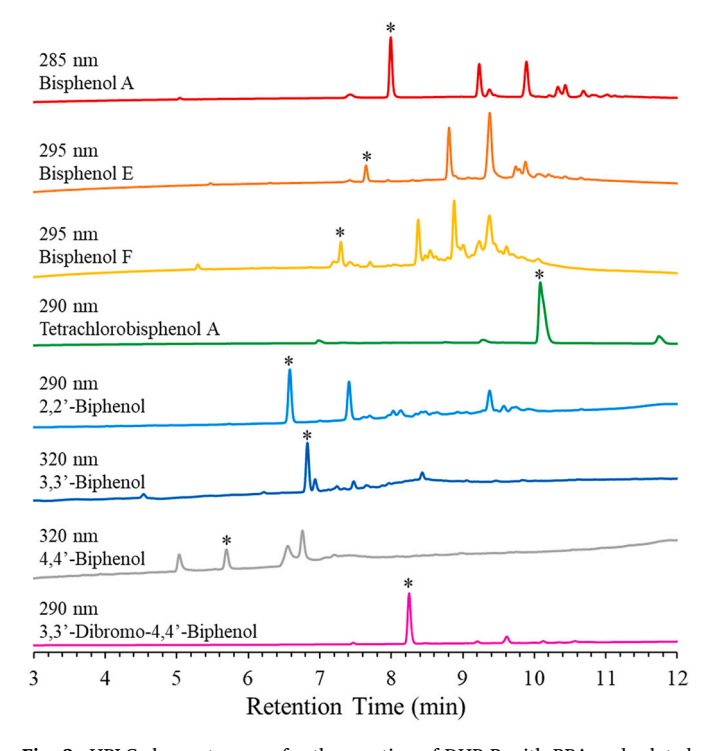


Fig. 2. HPLC chromatograms for the reaction of DHP B with BPA and related compounds in the presence of H_2O_2 . The reactions were monitored at the indicated wavelength. Optimized reaction conditions: [ferric DHP B] $=10~\mu\text{M}$, [substrate] $=[H_2O_2]=500~\mu\text{M}$, 5% MeOH/100 mM KP_i (v/v) at pH 8, 25 °C, 10 min. The reaction was quenched with the addition of excess of catalase. The asterisks denote the substrate.

Table 4BPA oxidation reaction products detected using GC–MS.

Product $t_{\rm R}$ (min)	m/z (% abundance)	Molecular Formula	Structure Assignment
24.32	134, 119, 105, 91, 77, 65, 51 (100, 80.6, 8.7, 30.2, 11.4, 12.4, 7.0)	C ₉ H ₁₀ O	но-
26.71	152, 137, 119, 107, 91, 77, 65, 51 (16.0, 100, 2.9, 4.5, 4.0, 6.1, 8.9, 2.8)	$C_9H_{12}O_2$	4-Isopropenylphenol HO——OH 4-(2-Hydroxypropan-2-yl)phenol
43.39	228, 213, 119, 107, 99, 91, 77, 65 (21.4, 100, 14.8, 3.6, 3.5, 7.6, 3.0, 3.9)	$\mathrm{C}_{15}\mathrm{H}_{16}\mathrm{O}_2$	HO BPA OH

77(11.4), 65(12.4), 51(7.0)] that matched with an authentic sample of 4-isopropenylphenol by GC-MS (Fig. S1), whereas the product at $t_{\rm R}=$ 26.7 min showed mass fragmentation patterns [152(16.0), 137(100), 119(2.9), 107(4.5), 91(4.0), 77(6.1), 65(8.9), 51(2.8)] that matched with an authentic sample of 4-(2-hydroxypropan-2-yl)phenol by GC-MS (Fig. S2). 4-(2-hydroxypropan-2-yl)phenol was also similarly identified by HPLC (Fig. S3), with a retention time ($t_R = 5.0 \text{ min}$) and UV-visible spectrum that were identical to the authentic sample, providing unequivocal evidence for the identity of this species as being formed from O atom incorporation into the cleavage product. Many more products were identified by LC-MS, as shown in Table 5. Even though the exact cleavage products that were observed from GC-MS (4-isopropenylphenol and 4-(2-hydroxypropan-2-yl)phenol) cannot be found in the LC-MS, monomer and dimer connected to the one of cleavage products (monomer + B, m/z 377.18 and dimer + B, m/z 603.28) were detected, which is believed to result from further oxidation of the cleavage product, in line with previous reports for heme enzymecatalyzed oxidation of BPA [15]. It is important to note that a previous study showed that as products of BPA oxidation, 4-isopropenylphenol and BPA oligomers exhibited a decrease in estrogenic activity [68].

3.3. Isotopically labeled oxygen studies

In order to determine the origin of the O atom that was incorporated in 4-(2-hydroxypropan-2-yl)phenol, labeling studies were performed with BPA (as a bisphenol representative substrate) employing $\mathrm{H_2^{18}O}$ and $\mathrm{H_2^{18}O}_2$ (98% and 90% $\mathrm{^{18}O}$ -enriched, respectively), and the results were subsequently analyzed by GC–MS and LC-MS (negative ion modes to yield the [M-H] $^-$ species). The background subtracted total ion

Table 5BPA oxidation reaction products detected using LC-MS (negative ion mode).

Product t_R (min)	m/z	Molecular Formula	Description
7.74	227.11	$C_{15}H_{16}O_2$	Monomer
8.72	377.18	$C_{24}H_{26}O_4$	Monomer + B
9.95	319.13	$C_{21}H_{20}O_3$	A
10.40	469.20	$C_{30}H_{30}O_5$	A + B
10.50	603.28	$C_{39}H_{40}O_{6}$	Dimer + B
10.57	453.21	$C_{30}H_{30}O_4$	Dimer – 2H
11.44	545.23	$C_{36}H_{34}O_5$	Monomer + A
11.77	679.31	$C_{45}H_{44}O_6$	Trimer – 4H

chromatograms (TICs) are shown in Figs. 3, S4 and S5. In the presence of unlabeled H₂O and labeled H₂¹⁸O₂, no significant increase in mass was observed [m/z 152.0 (Fig. 3C)], when compared with the results obtained from the reaction under unlabeled H₂O/H₂O₂ conditions [m/z 152.1 (Fig. 3A)]. However, the presence of labeled H₂¹⁸O and unlabeled H_2O_2 resulted in an increase of 2 Da in product [m/z 152.0, 26.4%; m/z154.1, 100% (Fig. 3B)], suggesting that incorporation of labeled oxygen was derived from a water molecule. The results obtained for the reaction employing both labeled $H_2^{18}O$ and $H_2^{18}O_2$ [m/z 152.0, 19.3%; m/z 154.0, 100% (Fig. 3D)] were virtually identical to those of the H₂¹⁸O/H₂O₂ reaction, providing strong evidence for O-atom incorporation exclusively from water (and not from hydrogen peroxide), and consistent with a peroxidase mechanism for BPA oxidation by DHP B yielding 2-(4hydroxypropan-2-yl)phenol. Additionally, further oxidation products were observed to contain ¹⁸O in reactions that only contained labeled water (Figs. S4 and S5).

According to the products obtained and ¹⁸O labeling studies using GC-MS and LC-MS, these results suggest that BPA oxidation proceeds via a radical-based peroxidase mechanism, which is in line with the results that radical scavengers were shown to inhibit substrate conversion. Based on the results above and past precedent with HRP [15], we propose the following mechanism for the oxidation of BPA in the presence of DHP and hydrogen peroxide (Scheme 1): H2O2-activated DHP oxidizes BPA to the corresponding phenoxy radical, with its position(s) at the ortho and para carbons consistent with the electron resonance shown. Coupling between two radicals causes a sterically hindered intermediate, which is followed by elimination of an isopropylphenol carbocation and formation of product A (MW = 320) (step i). As indicated in Table 5, species A has been detected in the product solution by LC-MS. The carbocation intermediate undergoes a nucleophilic substitution reaction with water to form product B (MW = 152), which was observed by GC-MS (step ii). The carbocation is also subjected to proton elimination producing product C (MW = 134; step iii), as also observed in our GC-MS studies.

Labeling studies were also performed with 2,2'-biphenol (as a biphenol representative substrate), as its oxidation products also exhibited O atom incorporation (Table S2). Studies employed H₂¹⁸O and H₂¹⁸O₂ (98% and 90% ¹⁸O-enriched, respectively), and the results were analyzed by LC-MS (negative ion mode to yield the [M-H] species). The background subtracted total ion chromatograms (TICs) are shown in Fig. S6 for the $\lceil \text{dimer} + 10 - 2H \rceil$ product, with the following observations: in the presence of unlabeled H_2O and labeled $H_2^{18}O_2$, no significant increase in mass was observed [m/z 385.10 (Fig. S6C)], when compared with the results obtained from the reaction under unlabeled H₂O/H₂O₂ conditions [m/z 385.10 (Fig. 3A)]. However, the presence of labeled $H_2^{18}O$ and unlabeled H_2O_2 resulted in an increase of 2 Da in product [m/z]385.10, 53.4%; m/z 387.10, 100% (Fig. S6B)], suggesting that incorporation of labeled oxygen was derived from a water molecule. The results obtained for the reaction employing both labeled H₂¹⁸O and $H_2^{18}O_2$ [m/z 385.10, 43.8%; m/z 387.10, 100% (Fig. S6D)] were virtually identical to those of the H₂¹⁸O/H₂O₂ reaction, consistent with Oatom incorporation exclusively from water (and not from hydrogen peroxide). The results shown here support a peroxidase mechanism for 2,2'-biphenol oxidation by DHP B, and are in-line with the labeling results observed for BPA oxidation.

3.4. Binding studies

The electronic absorption spectra of WT ferric DHP B in the presence of BPA and related compounds were monitored in 100 mM KP $_{\rm i}$ (pH 7) containing 5% (v/v) MeOH. No significant spectral changes were noted in the presence of bisphenol E, bisphenol F, 3,3'-biphenol and 4,4'-biphenol (data not shown), suggesting that these are either weak binding substrates, or that they do not bind in a manner that would lead to changes in the heme environment detectable by UV–visible spectroscopy. For BPA, tetrachlorobisphenol A and 3,3'-dibromo-4,4'-biphenol, their poor solubility limited the titration studies with WT DHP B, and these were therefore precluded for substrate binding studies.

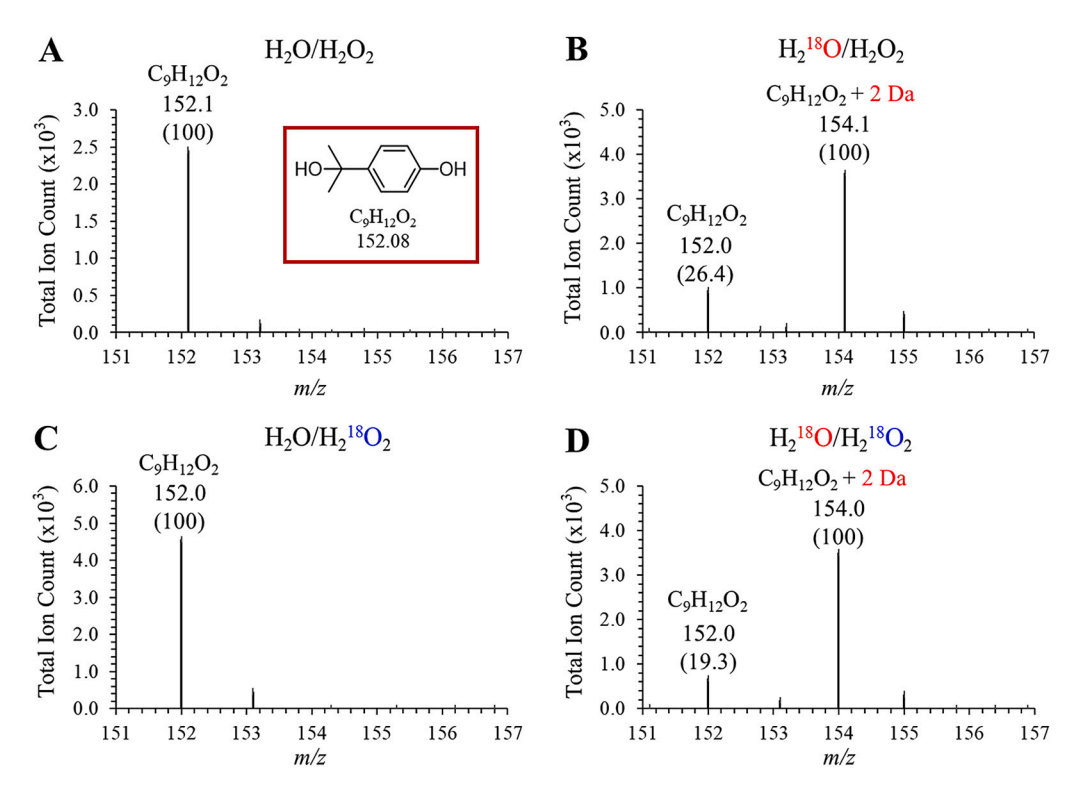


Fig. 3. Total ion chromatograms (TIC) obtained by GC–MS for the 2-(4-hydroxypropan-2-yl)phenol product observed in the oxidation reaction of BPA with DHP B: (A) H_2O/H_2O_2 , (B) $H_2^{18}O/H_2O_2$, (C) $H_2O/H_2^{18}O_2$, and (D) $H_2^{18}O/H_2^{18}O_2$. Reaction conditions: 10 μ M DHP, 500 μ M BPA, 500 μ M H_2O_2 , 5% MeOH /100 mM KP₁ (ν/ν), pH 8, 25 °C.

$$\begin{array}{c} DHP \\ H_2\mathbf{O}_2, H_2\mathbf{O} \end{array}$$

II)
$$H^{\circ}$$
 OH Substitution H° OH H° OH H° H° H° OH H° H°

III)
$$\stackrel{}{\longrightarrow}$$
 OH $\stackrel{}{\longrightarrow}$ Deprotonation $\stackrel{}{\longrightarrow}$ OH $\stackrel{}{\longrightarrow}$ (C, MW = 134)

Scheme 1. Proposed mechanism for the oxidation of BPA by H₂O₂-activated DHP yielding products A, B and C as identified by LC-MS and GC-MS studies.

Substrate binding studies were successfully conducted only with 2,2'-biphenol (Fig. S7) as it showed well-behaved optical difference spectra in the Q-band region compared to WT ferric DHP B upon titration (1–200 equiv). These optical changes allowed for the determination of the apparent substrate binding constant (K_d), which was calculated to be 61.7 μ M. Compared to the other single phenolic substrates, such as phenols [27,30,65,69], cresols [30] and guaiacols [29], 2,2'-biphenol showed a relatively strong binding affinity to DHP B (Table 6).

3.5. Stopped-flow UV-vis spectroscopic studies with BPA

Single and double mixing stopped-flow UV–vis spectroscopic methodologies were employed to investigate the oxidation of BPA (as a representative substrate) by DHP B. Single mixing experiments were conducted by preincubating DHP (i.e., DHP B(Y28F/Y38F), ferric DHP B, or oxyferrous DHP B) with BPA followed by the addition of $\rm H_2O_2$

Table 6 Dissociation constants (K_d) for substrate binding to ferric WT DHP B at pH 7.

Substrate	<i>K</i> _d (μM)	Ref.	Substrate	<i>K</i> _d (μM)	Ref.
2,2'-Biphenol Phenols	61.7 ± 2.3	a	Cresols p-Cresol	2682 ± 381	[30]
2,4-Dichlorophenol	29.3 ± 1.3	[69]	4-Me-o-cresol	309 ± 26	[30]
2,6-Dichlorophenol	$\begin{array}{c} 2400 \pm \\ 430 \end{array}$	[69]	4-Cl-o-cresol	130 ± 4	[30]
2,4,6- Trichlorophenol	208 ± 13	[70]	4-Br-o-cresol	86 ± 14	[30]
Pentachlorophenol	79 ± 9	[30]	4-NO ₂ -o- cresol	155 ± 5	[30]
4-Bromophenol	1150	[65]	Guaiacols		
2,4-dibromophenol	6.4 ± 0.6	[69]	o-Guaiacol	$\begin{array}{c} \textbf{14,712} \pm \\ \textbf{714} \end{array}$	[29]
2,6-dibromophenol	$\sim 7100 \pm \\3600$	[69]	4-Me- <i>o</i> - guaiacol	1433 ± 97	[29]
4-Nitrophenol	262 ± 23	[27]	4-Cl- <i>o</i> - guaiacol	493 ± 53	[29]
2,4-dinitrophenol	105 ± 21	[27]	4-Br-o- guaiacol	374 ± 42	[29]
4-nitrocatechol	40 ± 1	[27]	4-NO ₂ -o- guaiacol	1341 ± 26	[29]

^a This work.

(Figs. 4 and S9). Double mixing experiments were performed with $\rm H_2O_2$ -activated DHP (i.e., preformed either as Compound I [DHP B(Y28F/Y38F)] [40,41], Compound ES [26,33], or Compound II [47]) followed by their reaction with BPA (Fig. S10). For the majority of the studies described below, the data did not fit one-step/two species, two-step/three species or three-step/four species irreversible mechanisms, and as such, experimentally obtained spectra at selected time points detailed in the figure legends are shown.

3.5.1. Single mixing studies

3.5.1.1. Ferric DHP B(Y28F/Y38F) reactivity. Ferric DHP B(Y28F/Y38F) preincubated with 20 equiv. of BPA was reacted with 10 equiv. of $\rm H_2O_2$ at pH 8 (Fig. 4A). No formation of compound I was seen under these conditions, likely due to its immediate reduction in the presence of BPA substrate. Rather, a spectrum assigned to ferric DHP B(Y28F/Y38F) was initially observed [408 (Soret), 504, 543 (sh) and 645 nm, black; t = initial] [41], followed by formation of ferryl DHP B(Y28F/Y38F) [416 (Soret), 543 and 584 nm, red; t=1.6 s], and finally conversion to a ferric-like DHP B(Y28F/Y38F) [408 (Soret), 504, 543 (sh), 584 and 645 nm, blue; t=49.5 s] species, with the additional broad absorbance in the region of 300–350 nm being ascribed to product formation.

3.5.1.2. Ferric DHP B reactivity. ferric WT DHP B (10 μ M) preincubated with 20 equiv. of BPA was reacted with 10 equiv. of H₂O₂ at pH 8 (Fig. 4B). The ferric-like DHP B [412 (Soret), 542 and 588 nm, black; t = initial] spectrum converted to one that matched ferryl DHP B [420 (Soret), 546 and 589 nm, red; t=4.7 s] (i.e., Compound ES [26] or Compound II [47]), which subsequently underwent reduction back to the ferric state [412 (Soret), 542, 588 and 630 nm, blue; t=49.4 s] with the formation of products around 300–350 nm. The ferric WT DHP B spectrum at pH 8 containing 5% MeOH is shown in Fig. S8.

3.5.1.3. Oxyferrous DHP B reactivity. Previous studies have shown that oxyferrous DHP can be activated by H_2O_2 in the presence of a substrate [25,27–30,32], whereas in its absence, only a slight bleaching of the Soret band and/or long time scale conversion to Compound RH is observed [43,47]. Single mixing studies were conducted to investigate if BPA was also able to initiate this substrate-dependent activation of

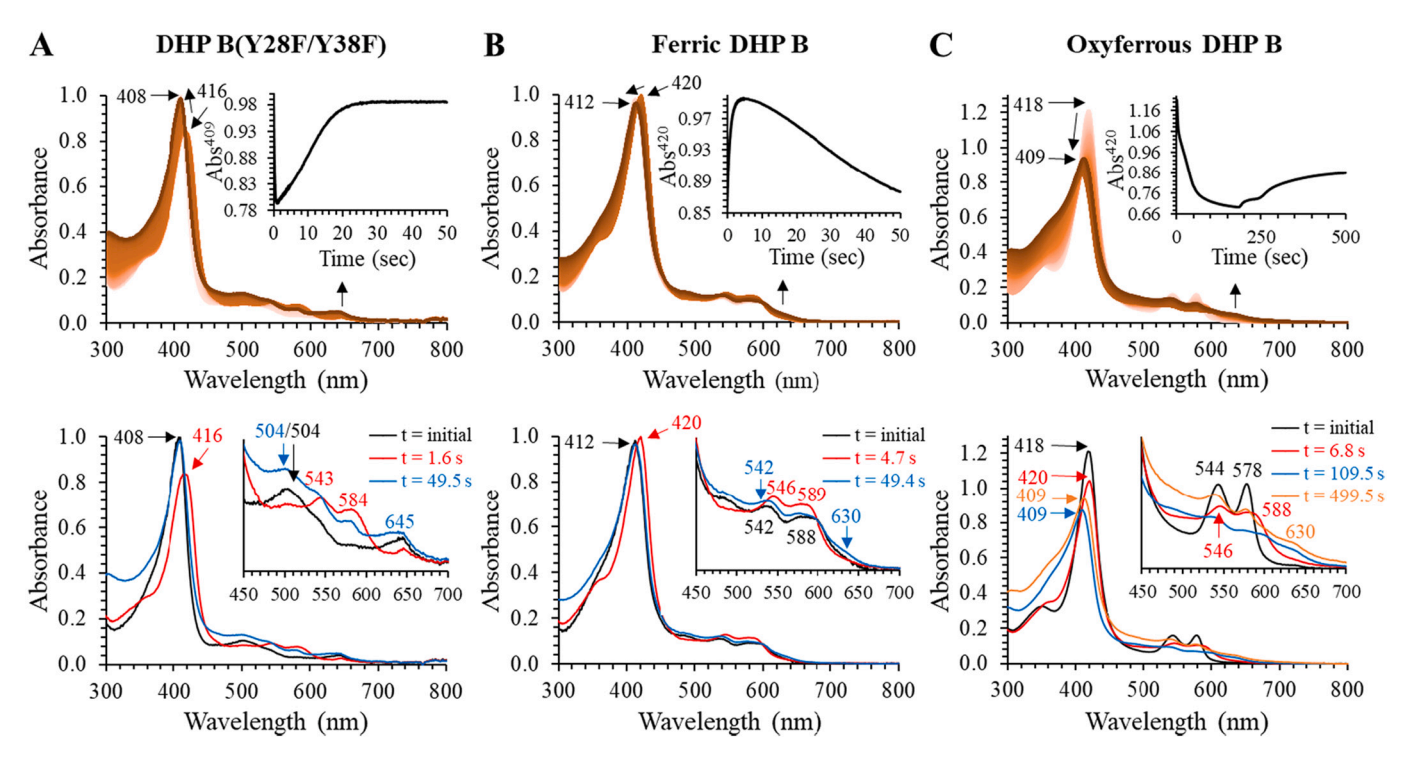


Fig. 4. Kinetic data for the reaction of H_2O_2 -activated DHP B with BPA at pH 8 and room temperature. (A) DHP B (Y28F/Y38F): *top panel*, stopped-flow UV-visible spectra of the single-mixing reaction between ferric DHP B (Y28F/Y38F) (10 μM) preincubated with 20 equiv. of BPA and reacted with 10 equiv. of H_2O_2 (900 scans over 50 s); inset: the single-wavelength (409 nm) dependence on time obtained from the raw data. *Bottom panel*, experimentally obtained spectra for DHP B (Y28F/Y38F) (black, t = 0 s), ferryl DHP B (Y28F/Y38F) (red, t = 1.6 s), and its reduction to a ferric-like species of DHP B (Y28F/Y38F) (blue, t = 49.5 s) with the formation of products. B) Ferric WT DHP B: *top panel*, stopped-flow UV-visible spectra of the single-mixing reaction between ferric DHP B (10 μM) preincubated with 20 equiv. of BPA and reacted with 10 equiv. of H_2O_2 (900 scans over 50 s); inset: the single-wavelength (420 nm) dependence on time obtained from the raw data. *Bottom panel*, experimentally obtained spectra for ferric DHP B (black, t = 0 s), ferryl DHP B (red, t = 4.7 s), and its reduction to ferric DHP B (blue, t = 49.4 s) with the formation of products. C) Oxyferrous WT DHP B: *top panel*, stopped-flow UV-visible spectra of the single-mixing reaction between oxyferrous DHP B (10 μM) preincubated with 20 equiv. of BPA and reacted with 10 equiv. of H_2O_2 (900 scans over 500 s); inset: the single-wavelength (420 nm) dependence on time obtained from the raw data. *Bottom panel*, experimentally obtained spectra for oxyferrous DHP B (black, t = 0 s), ferryl DHP B (red, t = 6.8 s), its reduction to a ferric-like species of DHP B (blue, t = 109.5.4 s) with the formation of products, and further reduction to an oxyferrous/ferric DHP B mixture (orange, t = 499.5 s). (For interpretation of the references to colour in this figure legend, the reader is referred to the web version of this article.)

oxyferrous DHP B. Oxyferrous WT DHP B (10 μ M) preincubated with 20 equiv. of BPA was reacted with 10 equiv. of H₂O₂ at pH 8 (Fig. 4C). It was observed that the oxyferrous form [418 (Soret), 544 and 578 nm, black; t = initial] initially oxidized to a ferryl-heme intermediate [420] (Soret), 546 and 588 nm, red; t = 6.8 s], which matched with the spectral features of the species formed when employing TCP [43,47], 4-nitrophenol [27], 5-bromoidole [28] and pyrrole [32] substrates (where the Compound II intermediate was observed). This ferryl species further converted to a ferric-like state [409 (Soret), 542, 588 and 630 nm, blue; t = 109.5 s] with the formation of products around 300–400 nm, ultimately resulting in a mixture of ferric and oxyferrous DHP B [409 (Soret), 544, 578 and 630 nm, orange; t = 499.5 s]. Relatedly, the reaction employing 4-Br-o-guaiacol [29] similarly formed the ferric enzyme and then reduced back to the oxyferrous enzyme, however, for 4-Br-o-guaiacol, the formation of Compound II prior to formation of the ferric enzyme was not observed.

Single mixing studies were repeated with 1 equiv. of BPA (Fig. S9) to investigate if BPA can act similarly as TCP [47], i.e., able to activate oxyferrous DHP to the Compound II form without conversion or decay to either the ferric enzyme or Compound RH. The following spectral changes were noted: oxyferrous DHP B [419 (Soret), 544 and 578 nm, black; t = initial] was converted to a ferryl-heme intermediate [420 (Soret), 546 and 588 nm, red; t=24 s], followed by a mixture of ferric and oxyferrous DHP [412 (Soret), 544, 578 and 634 nm, blue; t = 499.5 s] being observed. Overall, it was found that 1 equiv. of BPA was also able to activate oxyferrous DHP B toward reactivity with $\rm H_2O_2$ via a Compound II intermediate.

3.5.2. Double mixing studies

3.5.2.1. Compound I reactivity. Compound I was pre-formed in an initial mixing step of ferric DHP B (Y28F/Y38F) with 10 equiv. of $\rm H_2O_2$ in an aging line for 70 ms, which was then reacted with 20 equiv. of BPA at pH 8. The activated enzyme, Compound I [406 (Soret), 528, and 645 nm] [41], was not observed (Fig. S10A). Rather, a mixture of both ferric and ferryl DHP B [415 (Soret), 543 and 582 nm, black; t = initial] was the first spectrum recorded, and it suggested that Compound I was rapidly reduced by the substrate within the mixing time (1.5 ms) of the stopped–flow apparatus. The mixture of ferric and ferryl DHP B then converted to a ferric-like state [408 (Soret), 543 and 582 (sh) nm, red; t = 49.5 s] that further increased with product formation [408 (Soret), blue; t = 139.5 s]. The absorption of the reaction products made assignment of the Q-band features indeterminate.

3.5.2.2. Compound ES reactivity. Compound ES was pre-formed in an initial mixing step of ferric DHP B with 10 equiv. of $\mathrm{H}_2\mathrm{O}_2$ in an aging line for 433 ms [26], which was subsequently reacted with 20 equiv. of BPA at pH 8 (Fig. S10B). The activated enzyme, Compound ES [420 (Soret), 546 and 588 nm, black; t = initial] converted to a ferric-like state [410 (Soret), 543 and 630 nm, red; t=87 s] that further increased with product formation [409 (Soret), blue; t=499.5 s]. The absorption of the reaction products made assignment of the Q-band features indeterminate. Reduction of Compound ES to the ferric enzyme has been noted previously for most DHP substrates, including halophenols [26], haloindoles [28], pyrrole [32], nitrophenols [27], haloguaiacols [29] and

halocresols [30]. However, the product-driven reduction from ferric to oxyferrous DHP B was not observed here, similar to findings employing pyrrole [32], nitrophenol [27] and halocresol [30] substrates.

3.5.2.3. Compound II reactivity. Compound II was pre-formed in an initial mixing step of 10 equiv. of H_2O_2 with oxyferrous DHP B that was preincubated with 1 equiv. of 2,4,6-trichlorophenol [47] in an aging line for 7.84 s, which was reacted with 20 equiv. of BPA at pH 8 (Fig. S10C). Initially, the preformed Compound II [420 (Soret) 546 and 588 nm, black; t = initial] converted to a ferric-like state [409 (Soret), 540 and 630 nm, red; t=117 s] that became more pronounced with product formation [409 (Soret), blue; t = 499.5 s]. The absorption of the reaction products made assignment of the Q-band features indeterminate. Reduction of Compound II to the ferric enzyme has been noted previously for 2,4,6-trichlorophenol [26], 5-Br-indole [28], pyrrole [32], 4-nitrophenols [27], 4-Br-o-guaiacols [29] and 4-Br-cresol [30]. However, the further product-driven reduction of ferric DHP to the oxyferrous form was not observed here, similar to findings employing nitrophenol [27] and halocresol [30] substrates.

The main observations from these stopped-flow studies with BPA were as follows: (i) Compound I was rapidly reduced by BPA within the mixing time of the instrument to a mixture of ferric/ferryl DHP, ii) Compound ES and Compound II were reduced by BPA to ferric DHP, iii) BPA was found to activate oxyferrous DHP toward reactivity with $\rm H_2O_2$ via a Compound II intermediate, even at 1 equiv. BPA, similar to TCP, and iv) none of the BPA oxidation products were able to further reduce DHP to the oxyferrous state, which is a departure from the observed reactivity with quinone products formed upon oxidation of native substrates.

3.6. X-ray crystallographic studies of WT DHP B complexed with substrates

The binding of the bisphenol and biphenol substrates to DHP B was further elucidated by X-ray crystallography. The complexes were generated by substrate soaking of DHP B crystals, and using this method it was possible to obtain structures of complexes with BPE, BPF, as well as 2,2'-biphenol and 3,3'-biphenol. The crystals of the complexes were not found to affect the space group P212121 in which this protein typically crystalizes, with two protomers in the asymmetric unit as previously established [27,29,30,64,71-74]. The structures were determined at varying resolutions, from 1.3 Å for 3,3'-biphenol to 1.9 Å for 2,2'bisphenol, and the X-ray data collection and refinement parameters for these structures are presented in Table S3, while the selected distances relative to the heme and surrounding residues are given in Table 7. All of the substrates were found to bind in the same region where the single ring phenolic substrates have been shown to interact. The notable feature of the bisphenol and biphenol substrates is that they are larger (\sim 7 Å diameter) than most other previously characterized substrates that contain one ring having a diameter of approximately 3 Å, and with two phenolic rings, the presence of a hydroxyl group on both rings additionally affects their binding interactions within the heme binding cavity. To illustrate the span of the space of the binding pocket that is occupied by the double ring phenolic substrates, Fig. 5 shows the superposition of the BPE structure with the structures of two ligands that interact with two distinct regions of the binding cavity: i) the first ligand, 2,6-dichlorophenol (PDB 7M1L), binds very close to the heme γ edge (this substrate aligns very well with the first ring of BPE, as can be seen in the Fig. 5); and ii) the second substrate, 4-Br-o-cresol (PDB 6ONX), binds deep into hydrophobic space of the distal heme cavity above the $\boldsymbol{\alpha}$ edge of the cofactor (this substrate superposes better with the second ring of BPE). The longest span between these two single ring phenolic substrates is 6.8 Å, while the longest span between the two rings in BPE is 7.3 Å. Thus, these two single ring phenolic substrate binding regions define the span of the interaction possibilities within the distal pocket

Table 7
Selected distances (Å) for DHP B-substrate complex (protomer A).

	Bisphenol E	Bisphenol F	2,2'- Biphenol	3,3'- Biphenol
PDB Entry	8DOG	8DOH	8DOI	8DOJ
Substrate occupancy	100%	A: 50% B: 40%	90%	80%
H55 N ^E ···Ring 1 OH (substrate)	5.6	5.7 / 5.5	7.7	7.2
H55 N ^ε ···Ring 2 OH (substrate)	13.6	14.1 / 13.4	9.6	14.1
H55 N ⁶ ···Ring 1 OH (substrate)	3.8	4.0 / 3.6	7.1	5.4
H55 N ⁸ ···Ring 2 OH (substrate)	12.1	12.3 / 11.9	9.2	12.3
F21 C ^γ ···Ring 1 C ¹ (substrate)	5.8	5.7 / 5.9	5.3	4.8
F21 C ^γ ···Ring 2 C ¹ (substrate)	4.4	3.6 / 4.3	5.3	3.9
F21 C ^{\(\zeta\)} ···Ring 1 C ^{\(\zeta\)} (substrate)	4.2	4.4 / 3.8	6.4	4.8
F21 C ^ζ ···Ring 2 C ⁴ (substrate)	5	4.4 / 4.6	3.7	4.3
Fe···Ring 1 OH (substrate)	7.4	8.0 / 7.5	7.6	7.2
Fe···Ring 2 OH (substrate)	9.7	7.1 / 8.1	3.0	8.6
Fe···H55 N ^ε	10.3	10.3	10.5	10.5
Fe···H55 N ^δ	8.3	8.4	10.1	8.7
Fe···H89 N ^ε	2.2	2.2	2.2	2.1
Fe to pyrrole N plane	0.26	0.18	0.14	0.25

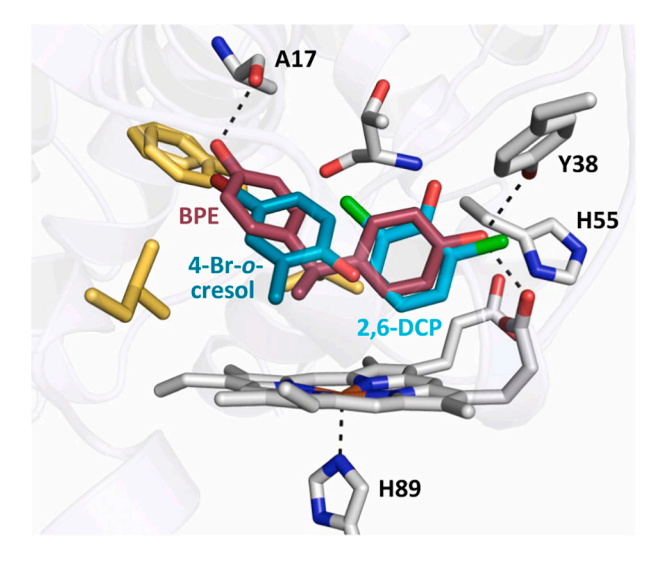


Fig. 5. Comparison of BPE-DHP B complex with other DHP B substrates. The bound BPE structure (PDB 8DOG), shown in dark red, is superposed on the 2,6-dichlorophenol bound complex (PDB 7M1L) shown in cyan, and the 4-Br-ocresol bound complex (PDB 6ONX) shown in teal. Only hydrogen bonding interactions involving the hydroxyl groups of BPE are presented. (For interpretation of the references to colour in this figure legend, the reader is referred to the web version of this article.)

binding space. In all these double ring phenolic structures, the H55 residue is present in the conformation facing outside of the binding pocket, and the two substrate rings occupy most of the distal pocket binding, as presented in Fig. 5.

The double ring phenolic substrates that were studied here belong to two groups: i) one that does not have much flexibility between two phenolic rings, represented by 3,3'-biphenol, shown in Fig. 6A, displayed together with the $2F_0$ - F_c electron density map for the substrate, and ii) one that has the two rings connected through an additional methylene bridging carbon atom, which allows more conformational

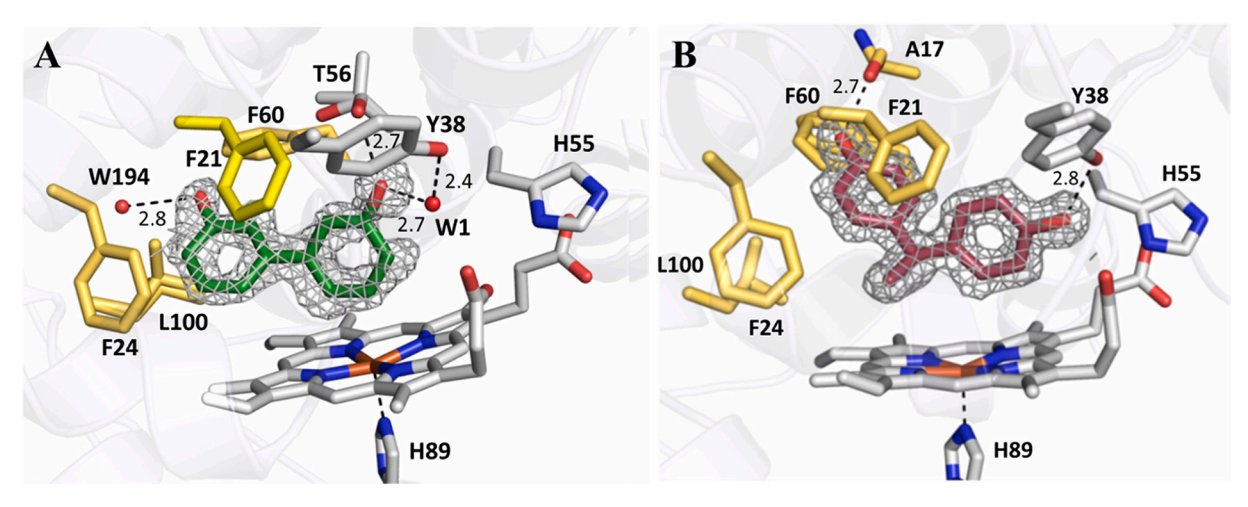


Fig. 6. Structural insight into the binding of DHP B with substrates (A) 3,3'-biphenol (PDB 8DOJ) and (B) BPE (PDB 8DOG). The binding site for the substrates is located above the heme molecule, and is surrounded by residues defining the heme distal cavity. Residues containing polar groups are shown in grey whereas hydrophobic residues are shown in yellow. Water molecules are displayed as red spheres. Hydrogen bonding interactions are presented as dashed lines between the hydroxyl groups of the substrates and their corresponding hydrogen bond partners. In the DHP complex with 3,3'-biphenol (panel A), there are two water molecules that are involved in hydrogen bonding interactions in the distal cavity. $2mF_0$ -DF_c electron density maps for the two substrates, contoured at 1.0 σ, are shown as grey mesh. (For interpretation of the references to colour in this figure legend, the reader is referred to the web version of this article.)

flexibility to the substrate. This group is represented by BPE, which is shown in complex with DHP B in Fig. 6B, displayed together with its $2F_0$ - F_c electron density map.

These ring connectivity features are one of the determining factors in the differences in binding of these two groups of substrates, in addition to having hydroxyl groups on both phenol rings in different relative positions. In substrates 2,2′-biphenol and 3,3′-biphenol, the binding site of the first ring is located close to the heme propionate entrance to the active site cavity, with their hydroxyl groups forming H-bonds with residues Y38 and T56, both of which are known to interact with the hydroxyl groups of some of the DHP substrates [29,30]. These binding interactions are presented in Fig. 7 where the two substrates are shown aligned to each other. The substrate H-bonding interactions are listed in Table 8. 2,2′-biphenol is bound just above the heme γ edge, perpendicular to the heme plane, with the ring C1-C6 edge being \sim 3–3.5 Å above the heme plane. The interaction is stabilized by its hydroxyl group forming H-bonds with residues T56 at 2.7 Å and Y38 at 3.4 Å. The

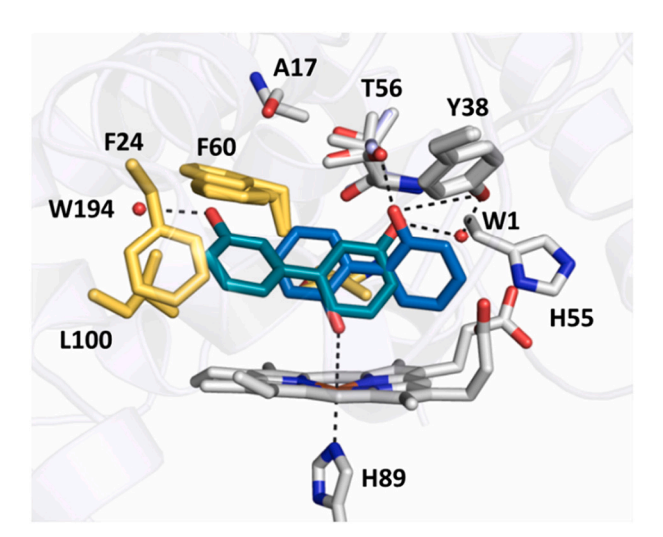


Fig. 7. Crystal structures of DHP B complexed with 2,2′-biphenol (blue, PDB 8DOI) and 3,3′-biphenol (teal, PDB 8DOJ). Hydrogen bonding interactions between the substrate and active site amino acids are shown. (For interpretation of the references to colour in this figure legend, the reader is referred to the web version of this article.)

hydroxyl group of the second ring appears to be interacting with heme iron at a distance of 3.1 Å. The second ring, although apparently in a π -stacking interaction with F35, seems to be more mobile than the first ring, as judged by less electron density and somewhat increased B factors associated with the upper part of the ring. Interestingly, for the efficient binding of 2,2'-biphenol that has the hydroxyl groups on the rings vicinal to each other, the second ring is flipped 180° relative to the first ring so that its hydroxyl group interacts with the iron center, as mentioned above, whereas the first ring is pointing up toward the hydroxyls of residues T56 and Y38. Moreover, the lack of flexibility between the two rings, as well as the hydroxyl group on the second ring, direct the substrate so that second ring is placed between residues L100 and F24, far from residue F60 that is usually associated with the placement of large hydrophobic substituents on the phenol ring [29,30]. 3,3'-biphenol, on the other hand, has the hydroxyl groups on the two rings more separated, and this distribution of polar functionalities causes the substrate to bind a little deeper into the binding pocket, facilitating the interaction of the second ring hydroxyl with a water molecule, W194, that was bound close to the carboxyl oxygen of residue L100 in this structure, while the hydroxyl group of the first ring interacts with residue Y38 via hydrogen bonding with a water molecule, labeled W1, bound close to this residue. In this arrangement, both hydroxyl functionalities of the substrate can establish hydrogen bonds in this largely hydrophobic environment. In addition, both of these substrates are engaged in π - π interactions with the phenyl rings of F21 and F35, thus strengthening their interactions in the distal pocket binding environment.

The binding of the bisphenol substrates, on the other hand, is affected by the flexibility of the orientation of the two phenyl rings relative to each other. The differences in binding of these two groups can be readily seen in Fig. 6 that individually shows the structures of 3,3′-biphenol (panel A), and BPE (panel B), as well as in Fig. 8 that shows these substrates superposed. The first phenolic ring of BPE is placed virtually perpendicular to the heme plane, close to the heme γ edge, at a distance of $\sim\!3.8$ Å from the heme plane, while the bridging methylene carbon is $\sim\!4$ Å from the heme plane. Due to the increased flexibility of the bisphenols over the biphenols, the second ring is positioned at an angle of $\sim\!114^\circ$ relative to the first ring. In this orientation, the second ring is close to residue F60, pushing the phenyl ring of this residue out to assume the alternate conformation that is commonly observed for the binding of substrates that contain bulky substituents on the ring [30].

Table 8Hydrogen bonds involving substrate hydroxyl groups and residues in the heme distal pocket (protomer A)^a.

Substrate	Distance (Å) to residue/ H_2O							
	H ₂ O	Y38	T56	Prop.D	H55 _{out}	A17 ^b	F21 ^b	Fe
BPE								
Ring1-OH		2.8		2.5	3.8			
Ring2-OH						2.7	3.5	
BPE								
Ring1-OH		$2.7/2.4^{\circ}$		$2.6/3.8^{c}$				
Ring2-OH						2.8		
2,2'-biphenol								
Ring1-OH		3.4	2.7					
Ring2-OH								3.1
3,3'-biphenol								
Ring1-OH	W1 ^d : 2.7	2.4 ^d	2.7					
Ring2-OH	W194 ^e : 2.8							

- ^a Hydrogen bond lengths are very similar for both protomers A and B, and only numbers for protomer A are listed as substrate occupancies are larger for protomer A.
- b Hydrogen bonding to main chain carbonyl (A17) or amide nitrogen (F21).
- ^c The two numbers refer to hydrogen bonds related to two substrate conformers.
- ^d First ring hydroxyl group of the substrate hydrogen bonds with water molecule W1, which in turn forms a H-bond with the hydroxyl group of residue Y38.
- ^e Hydroxyl group of the substrate ring 2 hydrogen bonds to a water molecule 194 located within the hydrophobic cavity.

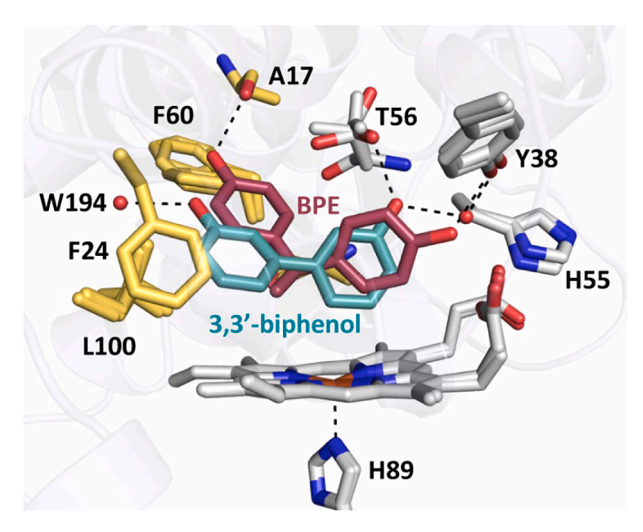


Fig. 8. Crystal structures of DHP B complexed with BPE (dark red, PDB 8DOG) and 3,3′-biphenol (teal, PDB 8DOJ). H-bonding interactions between the substrate and active site amino acids are shown. (For interpretation of the references to colour in this figure legend, the reader is referred to the web version of this article.)

The hydroxyl group of this ring is close to A17, and the interaction is stabilized by its hydrogen bonding with the main chain carbonyl of this residue.

Furthermore, the bisphenol substrates also differ in the substituents on the intervening carbon atom, and this feature affects the conformational scope in their binding to DHP. In the case of BPF, this carbon only has two hydrogens bound to it, and this seems to give the substrate more conformational freedom. This substrate is observed to bind in two conformations with occupancies of 0.4 and 0.5 in protomer A, and in one conformation with the occupancy of 0.6 in protomer B that is similar to the one observed for the protomer A conformation of 0.5 occupancy. The first conformation in protomer A is identical to the conformation observed for the BPE structure, shown in Fig. 9 with the BPE and BPF complex structures aligned with each other. The second conformation positions the second ring between residues F60 and L100, where the position of F60 can no longer be affected and where the hydroxyl group is no longer at a H-bonding distance to A17. The closest polar interaction would be with the main chain amide of F21 at 3.5 Å. In addition, this ring positioning seems to be very mobile since the overall electron density for this ring is diminished.

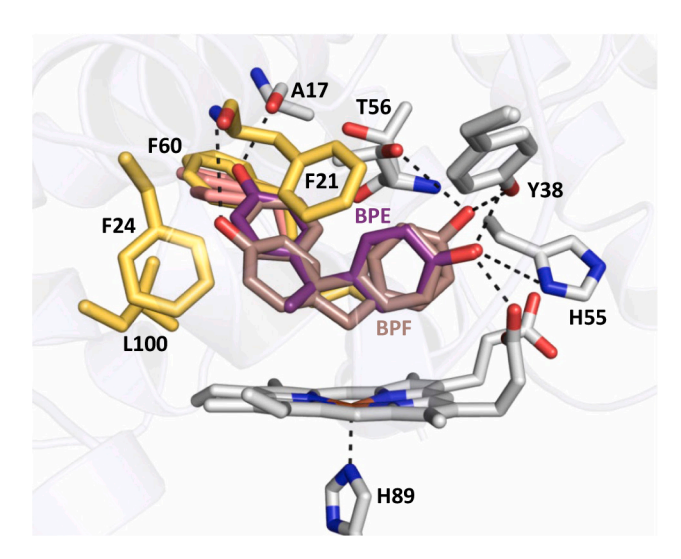
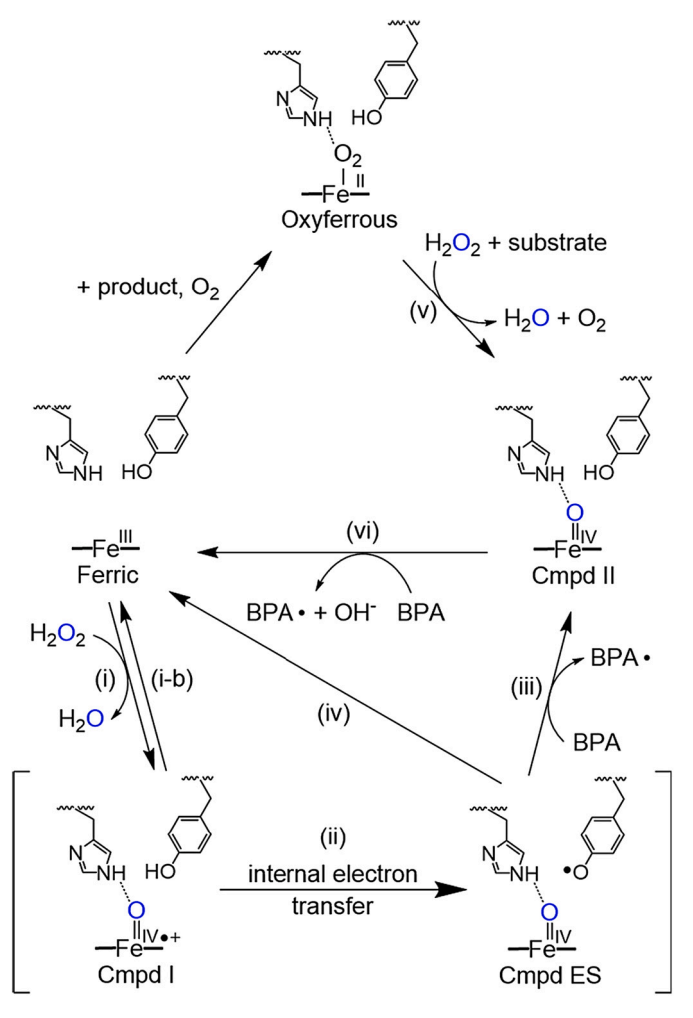


Fig. 9. Crystal structures of DHP B complexed with BPE (purple, PDB 8DOG) and BPF (light brown, PDB 8DOH). Hydrogen bonding interactions between the substrate and active site amino acids are shown. (For interpretation of the references to colour in this figure legend, the reader is referred to the web version of this article.)

3.7. Proposed peroxidase mechanism

On the basis of the previously established mechanisms for peroxidases (including dehaloperoxidase [24,26,29,30,44,45,47] and more traditional ones such as HRP [75]) and the results obtained above, we propose the following peroxidase catalytic cycle for the H₂O₂-dependent oxidation of BPA by ferric DHP B (Scheme 2): ferric DHP B reacts with 1 equiv. of H_2O_2 forming a two-electron oxidized ferryl species, either as Compound I (step i) or as Compound ES (step ii), which are subsequently reduced in the presence of BPA substrate to the ferric enzyme. The reaction could occur via either two consecutive one-electron oxidations [35] of BPA (steps iii and vi) or via a direct two electron oxidation of BPA (steps i-b and iv) based on the results from the stopped-flow studies. For two consecutive one-electron oxidations of BPA (step iii and vi), the reaction is likely to occur via a diffusible BPA phenoxyl radical that is subsequently oxidized by activated DHP, or through the disproportionation of two BPA radicals. The formation of diffusible radicals is consistent with radical-radical coupling reactions that produce cleavage products and oligomers [i.e., dimers, trimers, etc. (Tables 4 and 5)], as



Scheme 2. Proposed Peroxidase Catalytic Cycle for the Oxidation of BPA by DHP B.

well as the inhibition of the reaction in the presence of radical scavengers. Regardless of which pathway results in its formation, the oxyferrous form of the enzyme can be activated for peroxidase activity in the presence of $\rm H_2O_2$ and BPA substrate through a Compound II species (step v and vi). This proposed mechanism thus provides pathways for BPA oxidation by DHP starting from either the ferrous ('globin-like') or ferric ('peroxidase-like') oxidation states.

4. Conclusion

In summary, DHP has now been shown to possess an expanded substrate scope for peroxidase function. Previous studies have shown that DHP, a multifunctional catalytic globin, is able to catalyze the oxidation/degradation of single ring phenolic compounds. Here, we found that DHP can internally bind and catalyze the oxidation of double ring phenolic compounds, including BPA and related compounds (bisphenol E, bisphenol F, tetrachlorobisphenol A, 2,2'-biphenol, 3,3'biphenol, 4,4'-biphenol and 3,3'-dibromo-4,4'-biphenol). Among these substrates, it was found that the oxidation of BPA occurs via peroxidase pathway, as was confirmed by ¹⁸O-labeling studies that demonstrated that the O atom insertion into the products was from solvent water. Although there are extensive literature reports on the biodegradation of BPA by several different microorganisms or plants, DHP provides an example of the biodegradation of BPA by an invertebrate enzymatic pathway: namely, two cleavage products and oligomers with different oxidation degrees were identified by GC-MS and LC-MS. Given that BPA and related compounds are widely used in industry and are known

marine contaminants, our results demonstrate how these pollutants, either directly or indirectly (through their degradation or biotransformations resulting in metabolites), are impacted by, and can potentially impact, infaunal invertebrates and other marine organisms. Beyond this, however, it appears that *A. ornata*, a multifunctional globin, may be a promising system as a bioremediation catalyst through protein engineering such as heme cofactor modification or traditional mutagenesis, and it opens opportunities to explore other marine globins from benthic ecosystems for this potential.

Author statement

Dongju Yun was responsible for the biochemical assays and spectroscopic studies; Vesna de Serrano obtained the crystallographic results reported; Reza A. Ghiladi oversaw the project scope and experimental design, and all authors contributed to the writing and editing of the manuscript.

Declaration of Competing Interest

The authors declare that they have no known competing financial interests or personal relationships that could have appeared to influence the work reported in this paper.

Data availability

Data will be made available on request.

Acknowledgements

This project was supported by the National Science Foundation (CHE-2002954). This work was performed in part by the Molecular Education, Technology and Research Innovation Center (METRIC) at NC State University, which is supported by the State of North Carolina. X-ray diffraction data were collected at Southeast Regional Collaborative Access Team (SER-CAT) ID22 and BM22 beamlines at the Advanced Photon Source, Argonne National Laboratory. Supporting institutions may be found at www.ser-cat.org/members.html. Use of the Advanced Photon Source was supported by the U. S. Department of Energy, Office of Science, Office of Basic Energy Sciences, under Contract No. W-31-109-Eng-38.

Appendix A. Supplementary data

Supplementary data to this article can be found online at https://doi.org/10.1016/j.jinorgbio.2022.112020.

References

- A.T. Rigopoulos, V.F. Samanidou, M. Touraki, Development and validation of an HPLC-DAD method for the simultaneous extraction and quantification of bisphenol-a, 4-Hydroxybenzoic acid, 4-hydroxyacetophenone and hydroquinone in bacterial cultures of *Lactococcus lactis*, Pure Chem Sep. 5 (2018) 12.
- [2] S. Rodriguez-Mozaz, M.L. de Alda, D. Barceló, Analysis of bisphenol a in natural waters by means of an optical immunosensor, Water Res. 39 (2005) 5071–5079.
- [3] P.-P. Hao, Determination of bisphenol a in barreled drinking water by a SPE-LC-MS method, J. Environ. Sci. Health A 55 (2020) 697-703.
- [4] Z. Jiao, L. Chen, G. Zhou, H. Gong, X. Zhang, Y. Liu, X. Gao, Degradation of bisphenol a by CeCu oxide catalyst in catalytic wet peroxide oxidation: efficiency, stability, and mechanism, Int. J. Environ. Res. Public Health 16 (2019) 4675.
- [5] H. Okada, T. Tokunaga, X. Liu, S. Takayanagi, A. Matsushima, Y. Shimohigashi, Direct evidence revealing structural elements essential for the high binding ability of bisphenol a to human estrogen-related receptor-γ, Environ. Health Perspect. 116 (2008) 32–38.
- [6] J.C. O'Connor, R.E. Chapin, Critical evaluation of observed adverse effects of endocrine active substances on reproduction and development, the immune system, and the nervous system, Pure Appl. Chem. 75 (2003) 2099–2123.
- [7] M. Wang, X. Su, S. Yang, L. Li, C. Li, F. Sun, J. Dong, Y. Rong, Bisphenol a degradation by Fenton advanced oxidation process and operation parameters optimization, E3S Web Conf. 144 (2020) 01014.

- [8] C. Nadejde, M. Neamtu, V.D. Hodoroaba, R.J. Schneider, A. Paul, G. Ababei, U. Panne, Green Fenton-like magnetic nanocatalysts: synthesis, characterization and catalytic application, Appl. Catal. B 176-177 (2015) 667–677.
- [9] M. Deborde, S. Rabouan, P. Mazellier, J.-P. Duguet, B. Legube, Oxidation of bisphenol a by ozone in aqueous solution, Water Res. 42 (2008) 4299–4308.
- [10] X. Tan, Y. Wan, Y. Huang, C. He, Z. Zhang, Z. He, L. Hu, J. Zeng, D. Shu, Three-dimensional MnO2 porous hollow microspheres for enhanced activity as ozonation catalysts in degradation of bisphenol A, J. Hazard. Mater. 321 (2017) 162–172.
- [11] W.-D. Oh, L.-W. Lok, A. Veksha, A. Giannis, T.-T. Lim, Enhanced photocatalytic degradation of bisphenol A with Ag-decorated S-doped g-G3N4 under solar irradiation: performance and mechanistic studies, Chem. Eng. J. 333 (2018) 739-749
- [12] S. Ahmadzadeh, M. Dolatabadi, Modeling and kinetics study of electrochemical peroxidation process for mineralization of bisphenol A; a new paradigm for groundwater treatment, J. Mol. Liq. 254 (2018) 76–82.
- [13] H. Heidari, M. Sedighi, S.M. Zamir, S.A. Shojaosadati, Bisphenol A degradation by Ralstonia eutropha in the absence and presence of phenol, Int. Biodeterior. Biodegradation 119 (2017) 37–42.
- [14] E. Syranidou, S. Christofilopoulos, M. Politi, N. Weyens, D. Venieri, J. Vangronsveld, N. Kalogerakis, Bisphenol-A removal by the halophyte Juncus acutus in a phytoremediation pilot: characterization and potential role of the endophytic community, J. Hazard. Mater. 323 (2017) 350–358.
- [15] Q. Huang, W.J. Weber, Transformation and removal of bisphenol a from aqueous phase via peroxidase-mediated oxidative coupling reactions: efficacy, products, and pathways, Environ. Sci. Technol. 39 (2005) 6029–6036.
- [16] J.-H. Kang, Y. Katayama, F. Kondo, Biodegradation or metabolism of bisphenol a: from microorganisms to mammals, Toxicology 217 (2006) 81–90.
- [17] L. Pollock, A Practical Guide to the Marine Animals of Northeastern North America, Rutgers University Press, New Brunswick, 1998.
- [18] G.W. Gribble, Naturally occurring organohalogen compounds a comprehensive update, Springer, Vienna, 2010.
- [19] G.W. Gribble, The diversity of naturally occurring organobromine compounds, Chem. Soc. Rev. 28 (1999) 335–346.
- [20] G.W. Gribble, The natural production of organobromine compounds, Environ. Sci. Pollut. Res. Int. 7 (2000) 37–47.
- [21] M.W. LaCount, E. Zhang, Y.P. Chen, K. Han, M.M. Whitton, D.E. Lincoln, S. A. Woodin, L. Lebioda, The crystal structure and amino acid sequence of dehaloperoxidase from *Amphitrite ornata* indicate common ancestry with globins, J. Biol. Chem. 275 (2000) 18712–18716.
- [22] Y.P. Chen, S.A. Woodin, D.E. Lincoln, C.R. Lovell, An unusual dehalogenating peroxidase from the marine terebellid polychaete *Amphitrite ornata*, J. Biol. Chem. 271 (1996) 4609–4612.
- [23] L. Lebioda, M.W. LaCount, E. Zhang, Y.P. Chen, K. Han, M.M. Whitton, D. E. Lincoln, S.A. Woodin, An enzymatic globin from a marine worm, Nature 401 (1999) 445.
- [24] S. Franzen, R.A. Ghiladi, L. Lebioda, J. Dawson, Chapter 10 multi-functional hemoglobin dehaloperoxidases, in: Heme Peroxidases, The Royal Society of Chemistry, 2016, pp. 218–244.
- [25] S. Sun, M. Sono, J. Du, J.H. Dawson, Evidence of the direct involvement of the substrate TCP radical in functional switching from oxyferrous O₂ carrier to ferric peroxidase in the dual-function hemoglobin/dehaloperoxidase from *Amphitrite* ornata, Biochemistry 53 (2014) 4956–4969.
- [26] J. D'Antonio, E.L. D'Antonio, M.K. Thompson, E.F. Bowden, S. Franzen, T. Smirnova, R.A. Ghiladi, Spectroscopic and mechanistic investigations of dehaloperoxidase B from *Amphitrite ornata*, Biochemistry 49 (2010) 6600–6616.
- [27] N.L. McCombs, J. D'Antonio, D.A. Barrios, L.M. Carey, R.A. Ghiladi, Nonmicrobial nitrophenol degradation via peroxygenase activity of dehaloperoxidasehemoglobin from *Amphitrite ornata*, Biochemistry 55 (2016) 2465–2478.
- [28] D.A. Barrios, J. D'Antonio, N.L. McCombs, J. Zhao, S. Franzen, A.C. Schmidt, L. A. Sombers, R.A. Ghiladi, Peroxygenase and oxidase activities of dehaloperoxidase-hemoglobin from *Amphitrite ornata*, J. Am. Chem. Soc. 136 (2014) 7914–7925.
- [29] A.H. McGuire, L.M. Carey, V. de Serrano, S. Dali, R.A. Ghiladi, Peroxidase versus Peroxygenase activity: substrate substituent effects as modulators of enzyme function in the multifunctional catalytic globin Dehaloperoxidase, Biochemistry 57 (2018) 4455–4468.
- [30] T. Malewschik, V. de Serrano, A.H. McGuire, R.A. Ghiladi, The multifunctional globin dehaloperoxidase strikes again: simultaneous peroxidase and peroxygenase mechanisms in the oxidation of EPA pollutants, Arch. Biochem. Biophys. 673 (2019). 108079.
- [31] N.L. McCombs, T. Moreno-Chicano, L.M. Carey, S. Franzen, M.A. Hough, R. A. Ghiladi, Interaction of azole-based environmental pollutants with the Coelomic hemoglobin from *Amphitrite ornata*: a molecular basis for toxicity, Biochemistry 56 (2017) 2294–2303.
- [32] N.L. McCombs, T. Smirnova, R.A. Ghiladi, Oxidation of pyrrole by dehaloperoxidase-hemoglobin: chemoenzymatic synthesis of Pyrrolin-2-ones, Catal. Sci. Technol. 7 (2017) 3104–3118.
- [33] J. Feducia, R. Dumarieh, L.B. Gilvey, T. Smirnova, S. Franzen, R.A. Ghiladi, Characterization of dehaloperoxidase compound ES and its reactivity with trihalophenols, Biochemistry 48 (2009) 995–1005.
- [34] J. Du, X. Huang, S. Sun, C. Wang, L. Lebioda, J.H. Dawson, Amphirite ornata dehaloperoxidase (DHP): investigations of structural factors that influence the mechanism of Halophenol dehalogenation using "peroxidase-like" myoglobin mutants and "myoglobin-like" DHP mutants, Biochemistry 50 (2011) 8172–8180.
- [35] R.L. Osborne, M.K. Coggins, G.M. Raner, M. Walla, J.H. Dawson, The mechanism of oxidative halophenol dehalogenation by Amphitrite ornata dehaloperoxidase is

- initiated by H₂O₂ binding and involves two consecutive one-electron steps: role of ferryl intermediates, Biochemistry 48 (2009) 4231–4238.
- [36] N.L. McCombs, Unraveling the multiple enzymatic activities of the dehaloperoxidase-hemoglobin from Amphitrite ornata, Chemistry (2017). PhD.
- [37] T.L. Poulos, J. Kraut, The stereochemistry of peroxidase catalysis, J. Biol. Chem. 255 (1980) 8199–8205.
- [38] T.L. Poulos, Thirty years of heme peroxidase structural biology, Arch. Biochem. Biophys. 500 (2010) 3–12.
- [39] C.V. Popescu, T. Dinh, H. Chen, D. Miller, A. Washburn, A. McGuire, R. Dumarieh, J. D'Antonio, R.A. Ghiladi, Mössbauer studies of the ferryl, ferrous and ferric states of dehaloperoxidase from A. ornata, J. Inorg. Biochem. 234 (2022), 111867.
- [40] R. Davydov, R.L. Osborne, M. Shanmugam, J. Du, J.H. Dawson, B.M. Hoffman, Probing the oxyferrous and catalytically active ferryl states of *Amphitrite ornata* dehaloperoxidase by cryoreduction and EPR/ENDOR spectroscopy. Detection of compound I, J. Am. Chem. Soc. 132 (2010) 14995–15004.
- [41] R. Dumarieh, J. D'Antonio, A. Deliz-Liang, T. Smirnova, D.A. Svistunenko, R. A. Ghiladi, Tyrosyl radicals in dehaloperoxidase: how nature deals with evolving an oxygen-binding globin to a biologically relevant peroxidase, J. Biol. Chem. 288 (2013) 33470–33482.
- [42] M.K. Thompson, S. Franzen, R.A. Ghiladi, B.J. Reeder, D.A. Svistunenko, Compound ES of dehaloperoxidase decays via two alternative pathways depending on the conformation of the distal histidine, J. Am. Chem. Soc. 132 (2010) 17501–17510.
- [43] J. Du, M. Sono, J.H. Dawson, Functional switching of Amphitrite ornata dehaloperoxidase from O₂-binding globin to peroxidase enzyme facilitated by halophenol substrate and H₂O₂, Biochemistry 49 (2010) 6064–6069.
- [44] T. Malewschik, R.A. Ghiladi, Dehaloperoxidase: an enzymatic Swiss army knife, Coord. Chem. Rev. 441 (2021), 213976.
- [45] S. Franzen, M.K. Thompson, R.A. Ghiladi, The dehaloperoxidase paradox, Biochim. Biophys. Acta 2012 (1824) 578–588.
- [46] V. de Serrano, J. D'Antonio, S. Franzen, R.A. Ghiladi, Structure of dehaloperoxidase B at 1.58 A resolution and structural characterization of the AB dimer from *Amphitrite ornata*, Acta Cryst. D66 (2010) 529–538.
- [47] J. D'Antonio, R.A. Ghiladi, Reactivity of deoxy- and oxyferrous dehaloperoxidase B from Amphitrite ornata: identification of compound II and its ferrous-hydroperoxide precursor, Biochemistry 50 (2011) 5999–6011.
- [48] A. Castro-Forero, D. Jiménez, J. López-Garriga, M. Torres-Lugo, Immobilization of myoglobin from horse skeletal muscle in hydrophilic polymer networks, J. Appl. Polym. Sci. Symp. 107 (2008) 881–890.
- [49] V.N. Goral, A.D. Ryabov, Reactivity of the horseradish peroxidase compounds I and II toward organometallic substrates. A stopped-flow kinetic study of oxidation of ferrocenes, IUBMB Life 45 (1998) 61–71.
- [50] P. Chenprakhon, J. Sucharitakul, B. Panijpan, P. Chaiyen, Measuring binding affinity of protein-ligand interaction using spectrophotometry: binding of neutral red to riboflavin-binding protein, J. Chem. Educ. 87 (2010) 829–831.
- [51] Z. Otwinowski, W. Minor, Processing of X-ray diffraction data collected in oscillation mode, in: C.W. Carter Jr., R.M. Sweet (Eds.), Methods in Enzymology, Academic Press, New York, 1997, pp. 307–326.
- [52] W. Kabsch, XDS, Acta Crystallogr. D Biol. Crystallogr. 66 (2010) 125-132.
- [53] A.J. McCoy, R.W. Grosse-Kunstleve, P.D. Adams, M.D. Winn, L.C. Storoni, R. J. Read, Phaser crystallographic software, J. Appl. Crystallogr. 40 (2007) 658–674.
- [54] Collaborative Computational Project, The CCP4 suite: programs for protein crystallography, Acta Cryst. D50 (1994) 760–763.
- [55] G.N. Murshudov, A.A. Vagin, E.J. Dodson, Refinement of macromolecular structures by the maximum-likelihood method, Acta Cryst. D53 (1997) 240–255.
- [56] P.V. Afonine, R.W. Grosse-Kunstleve, N. Echols, J.J. Headd, N.W. Moriarty, M. Mustyakimov, T.C. Terwilliger, A. Urzhumtsev, P.H. Zwart, P.D. Adams, Towards automated crystallographic structure refinement with phenix, Refine Acta Cryst. D68 (2012) 352–367.
- [57] P.D. Adams, P.V. Afonine, G. Bunkoczi, V.B. Chen, I.W. Davis, N. Echols, J. J. Headd, L.W. Hung, G.J. Kapral, R.W. Grosse-Kunstleve, A.J. McCoy, N. W. Moriarty, R. Oeffner, R.J. Read, D.C. Richardson, J.S. Richardson, T. C. Terwilliger, P.H. Zwart, PHENIX: a comprehensive Python-based system for macromolecular structure solution, Acta Cryst. D66 (2010) 213–221.
- [58] P. Emsley, B. Lohkamp, W.G. Scott, K. Cowtan, Features and development of Coot, Acta Cryst. D66 (2010) 486–501.
- [59] V.B. Chen, W.B. Arendall 3rd, J.J. Headd, D.A. Keedy, R.M. Immormino, G. J. Kapral, L.W. Murray, J.S. Richardson, D.C. Richardson, MolProbity: all-atom structure validation for macromolecular crystallography, Acta Crystallogr D Biol Crystallogr 66 (2010) 12–21.
- [60] K. Kuśmierek, The removal of chlorophenols from aqueous solutions using activated carbon adsorption integrated with $\rm H_2O_2$ oxidation, React. Kinet. Mech. Catal. 119 (2016) 19–34.
- [61] J. Zhang, G.-B. Li, J. Ma, Effects of chlorine content and position of chlorinated phenols on their oxidation kinetics by potassium permanganate, J. Environ. Sci. 15 (2003) 342–345.
- [62] J. Regueiro, A. Breidbach, T. Wenzl, Derivatization of bisphenol a and its analogues with pyridine-3-sulfonyl chloride: multivariate optimization and fragmentation patterns by liquid chromatography/Orbitrap mass spectrometry, Rapid Commun. Mass Spectrom. 29 (2015) 1473–1484.
- [63] M. Jonsson, J. Lind, G. Merényi, Redox and acidity properties of 2,2'- and 4,4'biphenol and the corresponding phenoxyl radicals, J. Phys. Chem. A 106 (2002) 4758–4762.
- [64] L.M. Carey, R. Gavenko, D.A. Svistunenko, R.A. Ghiladi, How nature tunes isoenzyme activity in the multifunctional catalytic globin dehaloperoxidase from *Amphitrite ornata*, Biochim. Biophys. Acta 2018 (1866) 230–241.

- [65] M.K. Thompson, M.F. Davis, V. de Serrano, F.P. Nicoletti, B.D. Howes, G. Smulevich, S. Franzen, Internal binding of halogenated phenols in dehaloperoxidase-hemoglobin inhibits peroxidase function, Biophys. J. 99 (2010) 1586-1595
- [66] J. Zhao, J. Moretto, P. Le, S. Franzen, Measurement of internal substrate binding in dehaloperoxidase-hemoglobin by competition with the heme-fluoride binding equilibrium, J. Phys. Chem. B 119 (2015) 2827–2838.
- [67] J. Zhao, S. Franzen, Kinetic study of the inhibition mechanism of dehaloperoxidase-hemoglobin a by 4-bromophenol, J. Phys. Chem. B 117 (2013) 8301–8309.
- [68] T. Fukuda, H. Uchida, M. Suzuki, H. Miyamoto, H. Morinaga, H. Nawata, T. Uwajima, Transformation products of bisphenol a by a recombinant Trametes villosa laccase and their estrogenic activity, J. Chem. Technol. Biotechnol. 79 (2004) 1212–1218.
- [69] T. Malewschik, L.M. Carey, V. de Serrano, R.A. Ghiladi, Bridging the functional gap between reactivity and inhibition in dehaloperoxidase B from *Amphitrite ornata*: mechanistic and structural studies with 2,4- and 2,6-dihalophenols, J. Inorg. Biochem. 111944 (2022).
- [70] A.H. McGuire, When a hemoglobin acts as a catalytic enzyme: mechanistic studies of dehaloperoxidase, Chemistry (2020) 136. PhD.
- [71] L.M. Carey, K.B. Kim, N.L. McCombs, P. Swartz, C. Kim, R.A. Ghiladi, Selective tuning of activity in a multifunctional enzyme as revealed in the F21W mutant of

- dehaloperoxidase B from Amphitrite ornata, J. Biol. Inorg. Chem. 23 (2018) 209–219
- [72] M.F. Davis, H. Gracz, F.A. Vendeix, V. de Serrano, A. Somasundaram, S.M. Decatur, S. Franzen, Different modes of binding of mono-, di-, and trihalogenated phenols to the hemoglobin dehaloperoxidase from *Amphitrite ornata*, Biochemistry 48 (2009) 2164–2172.
- [73] T. Moreno-Chicano, A. Ebrahim, D. Axford, M.V. Appleby, J.H. Beale, A.K. Chaplin, H.M.E. Duyvesteyn, R.A. Ghiladi, S. Owada, D.A. Sherrell, R.W. Strange, H. Sugimoto, K. Tono, J.A.R. Worrall, R.L. Owen, M.A. Hough, High-throughput structures of protein-ligand complexes at room temperature using serial femtosecond crystallography, IUCrJ 6 (2019) 1074–1085.
- [74] T. Moreno-Chicano, L.M. Carey, D. Axford, J.H. Beale, R.B. Doak, H.M. E. Duyvesteyn, A. Ebrahim, R.W. Henning, D.C.F. Monteiro, D.A. Myles, S. Owada, D.A. Sherrell, M.L. Straw, V. Srajer, H. Sugimoto, K. Tono, T. Tosha, I. Tews, M. Trebbin, R.W. Strange, K.L. Weiss, J.A.R. Worrall, F. Meilleur, R.L. Owen, R. A. Ghiladi, M.A. Hough, Complementarity of neutron, XFEL and synchrotron crystallography for defining the structures of metalloenzymes at room temperature, IUCxJ 9 (2022) 610–624.
- [75] H.B. Dunford, Chapter 5 Heme Peroxidase Kinetics, in: Heme Peroxidases, The Royal Society of Chemistry, 2016, pp. 99–112.